Precambrian Research 278 (2016) 145–160

Contents lists available at ScienceDirect

Precambrian Research

journal homepage: www.elsevier.com/locate/precamres

Chemical and textural overprinting of ancient stromatolites: Timing, processes, and implications for their use as paleoenvironmental proxies

D.A. Petrash [a,*], L.J. Robbins [a], R.S. Shapiro [b], S.J. Mojzsis [c,d], K.O. Konhauser [a]

[a] Department of Earth and Atmospheric Sciences, University of Alberta, Edmonton, AB, Canada
[b] Geological and Environmental Sciences Department, California State University, Chico, CA, USA
[c] Collaborative for Research in Origins (CRiO), Department of Geological Sciences, University of Colorado, UCB 399, 2200 Colorado Avenue, Boulder, CO 80309-0399, USA
[d] Institute for Geological and Geochemical Research, Research Center for Astronomy and Earth Sciences, Hungarian Academy of Sciences, 45 Budaörsi Street, H-1112 Budapest, Hungary

ARTICLE INFO

Article history:
Received 3 October 2015
Revised 1 March 2016
Accepted 19 March 2016
Available online 26 March 2016

Keywords:
Paleoproterozoic
Superior Province
Animikie Basin
Gunflint Formation
Stromatolites
Rare earths and trace elements
geochemistry

ABSTRACT

Shale-normalized Rare Earth Element (REE_{SN}) patterns and transition metal abundances in banded iron formations (BIF) and shales have long been used as paleoenvironmental proxies to investigate the evolving geochemistry of Precambrian oceans. Apparent similarities between the REE_{SN} of modern stromatolites and contemporary seawater values also mean that some ancient stromatolites could record paleo-ocean chemistry. To test this hypothesis, we present comparative mineralogical, textural, and spectral analyses of multifurcate, silicified and iron oxide/carbonate-rich, stromatolites from the ca.1.88 Ga Gunflint Formation (Ontario, Canada). Previous studies show that these organo-sedimentary structures represent the initiation of shallow marine sedimentation in the Animikie Basin on the southern tip of the Superior Province. We present evidence that these structures were originally stabilized by aragonite and Mg-bearing carbonates. Fabrics indicative of stromatolite accretion under local hypersaline conditions are also present, with La anomalies suggestive of laterally variable freshwater runoff. The admixture of partially evaporated seawater and silica-oversaturated deep seawater led to pervasive silicification of metastable carbonates and preservation of less soluble early diagenetic carbonate cements. Bulk rock transition metal contents point to lateral variability and dissimilar partitioning and fractionation during mineral formation, yet Ce anomalies amongst samples are similar. Considering the pronounced differences between the REE partitioning between Fe oxyhydroxide precipitates and carbonates, our results point to hematite and siderite as secondary minerals that postdate the stabilization of these structures by carbonates and silica. Stratabound relations of the Fe-rich stromatolites with diabase sills and dikes indicate that the pore water fluids evolved towards a localized state of hematite and siderite oversaturation towards the Mesoproterozoic. If hematite and siderite are both early diagenetic phases, then the Ce anomalies of these stromatolites may be a poor measure of the redox conditions of the shallow areas of the Animikie Basin at the time of accretion.

1. Introduction

The quest to quantitatively constrain the dynamic evolution of paleo-redox states in Precambrian oceans has led to the hypothesis that the trace metal content of ancient stromatolites can be used as valid proxies for ancient ocean chemistry (e.g., Kamber and Webb, 2001; Van Kranendonk et al., 2003; Bolhar et al., 2004, Bolhar and Vankranendonk, 2007; Kamber et al., 2004; Planavsky et al., 2009; Riding et al., 2014). In such studies, emphasis is placed on relative abundances of various bioactive trace element concentrations as well as shale-normalized Rare Earth Element (REE_{SN}) distributions in bulk samples. This approach is seemingly warranted by the observation that contemporary stromatolite communities robustly record modern seawater compositions (Webb and Kamber, 2000; Kamber and Webb, 2007). Broad consensus is that REE_{SN} and some transition metal signatures of ancient stromatolites are useful in the pursuit of an interpretable record of ancient seawater chemistry (see Riding et al., 2014).

An inherent difficulty with such models, however, is that Holocene stromatolites were affected only by shallow burial diagenesis. As such, it remains unquantified to what extent a far more complex diagenetic history within their ancient analogues overprinted original chemical signatures. Mechanisms that might promote disruption of such primary chemical indicators in ancient

* Corresponding author.

http://dx.doi.org/10.1016/j.precamres.2016.03.010
0301-9268/

stromatolites include: diagenetic mobilization of trace metals; fractionation of transition elements and/or REE during secondary mineral precipitation; or contamination with metals derived from exogenous sources (e.g., Palmer, 1985; Elderfield and Pagett, 1986; Palmer and Elderfield, 1986; Sholkovitz and Shen, 1995; Bau and Dulski, 1996; Reynard et al., 1999; Shields and Stille, 2001; Johannesson et al., 2006). In this regard, it is reasonable to evaluate to what extent the low trace metal concentrations typically found in these ancient putative organo-sedimentary structures reflect a record of (albeit, poorly constrained) burial diagenesis and exhumation histories, rather than primary, marine-derived sources.

Under the generally oxygen-depleted conditions that accompanied Paleoproterozoic stromatolite accretion (e.g., Poulton et al., 2004), a number of trace elements are expected to have been variably enriched within minerals comprising these structures. This is because the redox sensitivity of transition metals and cerium, their preferential affinity for certain authigenic mineral phases, their complexation behavior in the presence of reactive microbial biomass, and local scale paleoenvironmental factors, determined the magnitude of elemental enrichment in the different mineral phases. To investigate these various possibilities, we compared the textural, spectroscopic, and bulk-rock chemical signatures (transition metal and REE_{SN} abundances) of stromatolites of the Gunflint Formation from the region of Thunder Bay, Ontario, Canada (Fig. 1). It was previously recognized that these stromatolites are pervasively silicified even if they were essentially unmetamorphosed, which, in part, explains their remarkable microfossil content (Barghoorn and Tyler, 1965; Awramik and Barghoorn, 1977). It is also highly significant that their accretion occurred at a time in the evolution of marine chemical redox between the purported transition from largely ferruginous to sulfidic bottom water conditions (Poulton et al., 2004).

With regard to stromatolites thus far described from Archean-Proterozoic terranes, replacement of primary carbonates can range from slight to extensive, either by other carbonates (e.g., siderite, ankerite, calcite) or by non-carbonate minerals (e.g., amorphous silica). The sequence of events linked to the replacement process may be predictable, and in this regard, paragenetic relations between the cherty matrix (recrystallized amorphous silica) and dolomite offer insights into establishing the time during which silicification of the carbonates occurred (Dapples, 1979). Our goals here were to investigate the nature of silicification in the peritidal carbonates of the Gunflint Formation, with particular emphasis on the conditions necessary for silica permineralization. This will help elucidate any diagenetic bias on the bulk trace metal signatures of the secondarily silicified early diagenetic carbonate minerals. Conclusions drawn from this study are discussed in terms of the applicability of bulk-rock analyses of stromatolite samples to evaluate paleoceanographic conditions in deep geological time.

2. Geological background

Rocks that comprise the sedimentary successions of the 1.88 Ga Gunflint Formation were deposited uncomformably on deformed Neoarchean greenstone-granite basement rocks of the Superior Province, and within the southward-thickening domain of the Animikie Basin (e.g., Pufahl, 1996; Fralick et al., 2002; Jirsa and Fralick, 2010). Following earlier stratigraphic studies (i.e., Broderick, 1920), Goodwin (1956) subdivided this formation into four members: the Basal Conglomerate, the Lower and Upper Cherty Member(s), and the Upper Limestone. With minor modifications, these terms remain in use today. The ~120 m thick formation crops out nearly continuously from Gunflint Lake on the Minnesota–Ontario border

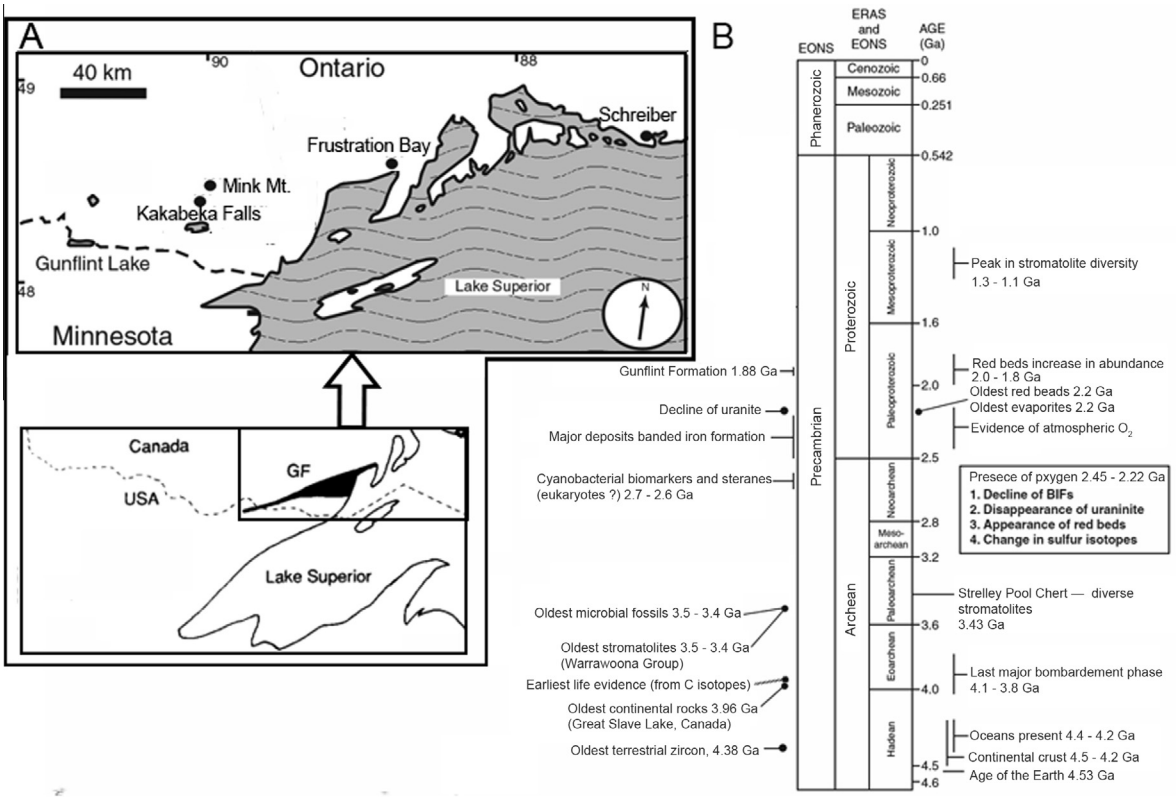

Fig. 1. Location of the stromatolite occurrences studied here. On the right, the Gunflint Formation and its chronostratigraphic relevance within the general context of the oxygenation of the Earth's atmosphere and evolution of primitive life (After Taylor and Taylor, 1993; Farquhar et al., 2011; Mojzsis et al., 2014).

to the east of Thunder Bay (Fralick, 1989). A geochronological investigation of a euhedral zircon population from the Upper Cherty Member yielded a U-Pb isochron age of 1878 ± 1.3 Ma interpreted to define the depositional age of this stratigraphic member (Fralick et al., 2002).

We focus on stromatolites collected from the very base of the Lower Cherty Member that directly overlies the basal conglomerate. Relative to the other lithofacies of the Gunflint, this member represents the shallowest shoreward depositional facies of the succession (Winter and Knauth, 1992). In his pioneering work, Goodwin (1960) further subdivided the Lower Cherty Member into the following set of lithofacies: "algal chert" (i.e., stromatolites), tuffaceous shale, taconite, and banded chert-carbonates. At about the same time, Moorehouse (1960) pointed out that the Lower Cherty Member exhibits complex lateral variations of stromatolitic silicified grainstones, BIF, and shale microfacies: he further divided the unit into eleven distinct lithofacies to account for these differences. The lateral and vertical transition of lithofacies in the Gunflint superficially resembles shallow marine mixed clastic-carbonate depositional systems. Thus, it is thought to represent two marginal depositional cycles controlled by relative sea-level changes (Fralick and Barrett, 1995; Pufahl and Fralick, 2000).

The laminar internal structure of the stromatolites is defined by the presence of (dark) kerogen and/or iron oxides (Moreau and Sharp, 2004). Exceptionally well-preserved microfossils were first documented by Barghoorn and Tyler (1965) and Cloud (1965) from the Gunflint rocks. The microfossils may be coated with iron oxides, and have been interpreted to represent the remains of cyanobacteria (e.g., Awramik and Barghoorn, 1977) or chemolithotrophic Fe-oxidizing bacteria (e.g., Knoll, 2003; Planavsky et al., 2009). Understanding these rocks is important because both the quality and quantity of Gunflint microfossil forms are the benchmark against which all other putative microscopic traces of early life are compared (Awramik and Barghoorn, 1977; Lowe, 1983; Schopf and Packer, 1987; Nudds and Selden, 2008; Planavsky et al., 2009; Wacey et al., 2012).

An early diagenetic silica permineralization process occurred shortly after stromatolite accretion to account for the exceptional preservation of the small microbial cell structures (Hesse, 1989; Knauth, 1994; Moreau and Sharp, 2004). The permineralization process probably involved the interaction of biofilms with seawater that was supersaturated at that time with respect to silica (i.e., Konhauser and Phoenix, 2001; Konhauser et al., 2004, 2005; Maliva et al., 2005). Other Precambrian stromatolites initially formed by processes of carbonate accretion, however, with the chert representing a secondary mineral phase formed during diagenesis (Buick and Dunlop, 1990; Grotzinger, 1994). Such stromatolites, typically accreted in the peritidal zone, are characterized by the presence of unreplaced carbonates and the preservation of inclusions and ghosts of carbonate precursors, also with pseudomorphs and inclusions of evaporites (Maliva et al., 2005, their Table 1).

3. Samples and methods

3.1. Samples

Samples from the Lower Gunflint Formation were collected in the Thunder Bay area. Locations for our collections occur along the northern shore of Lake Superior, at the Schreiber Channel Provincial Nature Reserve (Awramik and Barghoorn, 1977; Lanier, 1989), and the Frustration Bay locality (Awramik and Barghoorn, 1977). The Frustration Bay samples were provided by Dr. Stanley Awramik (University of California at Santa Barbara). At the Schreiber Channel locality, we used previously collected stromatolitic cherts containing ooidal/peloidal intraclasts. Specimens came from unattached black chert cobbles found offshore, adjacent to the protected outcrop. For comparison purposes, we also sampled laminar hematite-rich digitate stromatolitic rocks from the Upper Cherty Member exposed at Mink Mountain (Planavsky et al., 2009; Shapiro and Konhauser, 2015) and a section of a large hemispheroid dome near Kakabeka Falls.

3.2. Methods

Petrographic thick- (250 μm) and thin-sections (30–40 μm) were systematically analyzed by standard and blue fluorescence petrography, as well as by Scanning Electron Microscope coupled to an Energy Dispersive Spectrometer (SEM-EDS) at the University of Alberta. These analyses were conducted on the petrographic sections and freshly broken samples, respectively. For descriptions of the quartz textures, we follow the terminology of Folk (1974). Accordingly, we used microquartz to refer to equant quartz crystals less than 20 μm in diameter, and megaquartz as that material with a crystal size greater than ~20 μm. Chalcedony is used herein for microcrystalline quartz with parallel- or radial-fibrous extinction, irrespective of the sign of elongation. Chert is used for any aggregate consisting of microquartz, megaquartz and/or chalcedony. Silica is a blanket term for any precipitate with the same chemical composition as quartz (e.g., Simonson, 1987). For the description of dolomite/ankerite mineral textures, we followed the general scheme for naming these textures as outlined by Sibley and Gregg (1987).

Bulk-rock minor and trace elemental concentrations were determined at the University of Alberta. Initially a 0.2-g (dry

Table 1
Trace metal concentrations (ppm) and mineralogical and morphological features of the stromatolite samples.

Sample name and locality	V	Cr	Mn	Fe	Co	Ni	Cu	Zn	Mineralogy/description
Frustration Bay (FB)									
FB74g1	9.0	0.7	2,190	14,778	4.2	7.3	1.6	2.3	Silicified multifurcate stromatolites and centimeter-scale hemispheroids
FB74g1	10.2	1.1	2,351	17,076	4.4	7.6	2.2	3.0	with ankerite, pyrite, and minor fine crystalline dolomite
A.2-75	11.3	7.1	4,992	28,608	12.6	62.4	22.4	95.5	
Schreiber (Sch)									
Sch 1-2-1	<DL	0.4	36	557	0.6	0.7	5.7	3.8	Silicified multifurcate stromatolites with pyritized ooids/peloids. Ankerite
Sch 1-2-1	<DL	0.5	36	563	0.6	0.7	5.8	3.4	and minor fine crystalline dolomite
Sch 1-4-1	<DL	0.3	32	491	0.5	0.6	2.2	1.5	
Mink Mountain (MM)									
MkM3	3.9	2.0	623	14,737	1.7	1.2	6.2	11.2	Silicified hematite/siderite-rich multifurcate stromatolite
MkM4	2.7	2.6	938	16,058	1.2	1.6	3.7	7.7	
Kakabeka Falls									
Kaf 2-1	20.4	1.7	3,436	53,823	8.2	7.2	27.2	4.3	Large silicified hemispheroidal stromatolite with ankerite and calcite
Kaf 2-2	1.92	0.4	2,681	28,333	3.0	0.5	16.0	6.5	

weight) rock sample was digested in a platinum crucible with a solution of concentrated HNO_3 (2 mL) and HF (8 mL) to near dryness; subsequently a second addition of concentrated HCl (5 mL) and HNO_3 (5 mL) was made and again the mixture was evaporated to near dryness. The residue was then dissolved in 10 mL of 8 N HNO_3 and diluted to ~20 mL with 8.8 mL ultrapure water and 0.1 mL HNO_3. A 0.1 mL of a Br, In, and Sc spike was added. Samples were analyzed on an Perkin Elmer Elan6000 Inductively Coupled Plasma Quadrupole Mass Spectrometer (ICPQ-MS) under the following operating conditions: RF power = 1200 W; dual detector mode; blank subtraction performed subsequent to internal standard correction; unit of measurement is cps (counts per second); auto lens on; use of 4-point calibration curves (0, 0.25, 0.50, and 1.00 ppm for Ca, Mg, and Fe; 0.005, 0.010, and 0.020 ppm for the remaining elements); sample uptake rate (using a peristaltic pump) was ~1 mL; sample analysis consisted of 35 sweeps/reading, 1 reading/replicate and 3 replicates; dwell times were 10 ms for Mn, and 20 ms for the remaining elements; and total integration times (dwell time × number of sweeps) were 350 ms for Mn, and 700 ms for the remaining elements (Table 1). External reproducibility, based on repeated analysis of international whole rock standard (Granodiorite, Silver Plume, Colorado, GSP-2) is 5–10% (2σ level) for most elements. Internal standards for Bi, Sc and In were also used. Determined REE data were corrected using both off-line and on-line correction methods for interferences of BaO on Eu and NdO on Tb (e.g., Cheatham et al., 1993).

Following standard procedures, the La and Ce anomalies and measures of REE fractionation (i.e., (La/Yb), (Pr/Yb), (Nd/Yb), and (Gd/Yb)) were normalized against Post Archean Australian Shale (PAAS; Nance and Taylor, 1976; Taylor and McLennan, 1985). Normalization values (in ppm) for the REEs are: La (38), Ce (80), Pr (8.9), Nd (32), Sm (5.6), Eu (1.1), Gd (4.7), Tb (0.77), Dy (4.4), Ho (1.0), Er (2.9), Tm (0.4), Yb (2.8), and Lu (0.43). To evaluate for anomalous REE values, we used the approach developed by Bau and Dulski (1996) which prevents interpretations based on abnormal absolute concentrations of neighboring elements. For instance, the enrichment or depletion of Ce relative to La and Nd is widely used as a tracer for paleomarine redox conditions (Derry and Jacobsen, 1990; Bau and Möller, 1993; Shields and Stille, 2001). When only spider plots are used, however, the presence of Ce anomalies can be complicated by anomalous abundances of La.

Veizer et al. (1992) previously observed that the distribution of elements, such as Mn, Zn, and Y in Paleoproterozoic shelf sequences, is largely controlled by the carbonate fraction. To map the spatial distribution of yttrium at the scale of our digitate stromatolite samples, we employed synchrotron-based *in situ* micro-X-ray fluorescence (μXRF). These measurements were performed on the VESPERS microprobe beamline 07B2-1 at the Canadian Light Source (CLS) in Saskatchewan, and the 20ID-B beamline at the Advanced Photon Source (APS), Argonne National Laboratory (Illinois, USA). For both beamlines, the excitation energy was tuned at 20.2 keV, and a flux of 10^{10}–10^{11} photons-per-second was micro-focused over an analytical area of ~30 μm^2 using Kirkpatrick-Baez (KB) mirrors. For both beamlines, the resulting fluorescence spectra were measured using a 4 element Vortex multi-element Si drift detector located 90° to the incident beam in the direction of the polarization, and the detector calibrated to ~30 eV per channel. Spatially resolved X-Ray Diffraction analyses (2D-XRD) were used to obtain small-scale mineralogical information. The experimental geometry was corrected and 2θ calibration done by measuring the reflection patterns of LaB_6 (NIST, SRM 660b). Calibration of the 2d-spacing of the targeted mineral was done by using the d_{101} peak of quartz.

Yttrium abundance was used to infer the distribution of REE for two reasons. Firstly, its $K\alpha_1$ emission line is at 14.9 keV, and thus within the detectable range of our synchrotron analyses (~5.5–20.0 keV). In contrast, the other lanthanides have $K\alpha_1$ emission that range from 34.7 to 54.0 keV. This would mean that their detection would require tuning the instrument to much higher energies that are detrimental for determining the distribution of first row transition metals. Secondly, it is expected that the distribution of Y with the solid phases present in our samples, should be similar to Ho, and for that matter other HREEs. This is due to their similar complexation behavior (e.g., Huang, 2010).

4. Results

4.1. Petrography and mineralogy

Detailed petrological descriptions of the stromatolitic rocks from the Gunflint Formation have a long history. Earlier studies reported fine-scale petrographic features reminiscent of microbial cellular structures (e.g., Barghoorn and Tyler, 1965; Awramik and Barghoorn, 1977; Moreau and Sharp, 2004), silica cements (e.g., Simonson, 1987; Simonson and Lanier, 1987; Marin et al., 2010, 2012), coated grains (e.g., Simonson, 1987; Lanier, 1989), and pyrite (e.g., Tyler and Barghoorn, 1963; cf. Papineau et al., 2005). Yet, studies of the carbonate fraction, and the possibility for some of the silica cements to be a replacement product after carbonates (e.g., Ricketts, 1983; Grotzinger and Read, 1983; Grotzinger, 1986; Hofmann and Jackson, 1987; Buick and Dunlop, 1990), have received less attention (but see Markun and Randazzo, 1980; Sommers et al., 2000).

The stromatolite laminae from the Schreiber (Sch) and Frustration Bay (FB) outcrops contain an amorphous, dark-brown, organic-rich, silica matrix (Fig. 2A, B), which often includes fine euhedral to subhedral pyrite crystals that are typically 4–8 μm across (Fig. 2C–E). The pyrite may exhibit pyritohedral and octahedral morphologies, but cubic forms are more frequent. Individual pyrite crystals can reach 12–14 μm in size (Fig. 2D). The larger pyrite grains are concentrically zoned (Fig. 2E). In samples from FB, pyrite accounts for up to 6% of the bulk mineralogy. The stromatolitic Sch samples are relatively less abundant in pyrite (~3%), but the walls of some ooids can be pervasively replaced by pyrite (Fig. 2F–G). This result contrasts with observations made on the correlative, but stratigraphically higher, Mink Mountain locality (MM), where ooids are hematitic (Fig. 2H) and pyrite is generally absent (i.e., Planavsky et al., 2009; Shapiro and Konhauser, 2015). The primary porosity between peloid/ooid allochems is typically cemented by microquartz and megaquartz. Microquartz also comprises an isopachous cement infilling the original fenestral porosity (Figs. 2H and 3A–E).

In the Sch and FB locations, embedded within the isopachous cherty cement are fine (30–40 μm) rhombohedral crystals, which may also form mosaics within a microcrystalline silica matrix. High magnification SEM analyses of these cements reveal that the coarse rhombohedral crystals exhibit conchoidal fractures; they are silicified carbonates (Fig. 4B). When observed under blue light excitation, a first generation of microquartz cement surrounding the rhombs shows a dull luminescence with bright luminescent spots indicative of punctual accumulations of kerogen. The boundaries of the euhedral rhombs also display this characteristic bright luminescence (Fig. 4C), and these rhombohedral crystals are often in apparent optical continuity with the chert (Fig. 4D).

A second generation of radial-fibrous (or botryoidal) chalcedony cement infills the voids within the structures (Figs. 4D and 5A, B). This cement resembles the so-called submarine 'fan druse' as described by Shinn (1969) in the Persian Gulf, or 'spherulitic cement' described by Schroeder (1972) in Bermuda. The botryoidal chalcedony is length-slow as tested by insertion of the 550-nm full wave compensator (gypsum retardation plate) (i.e., it exhibits a

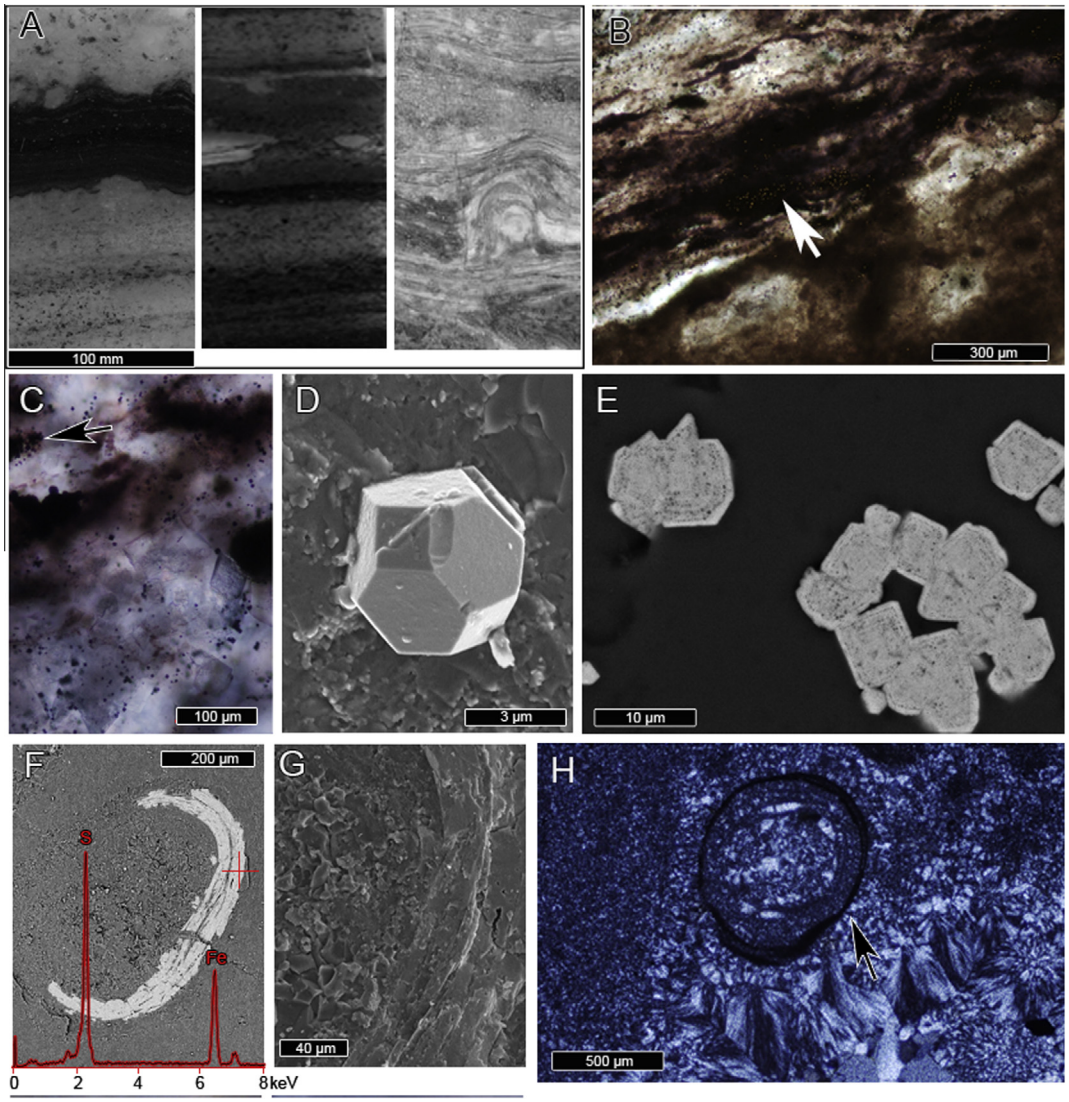

Fig. 2. Textural features of the stromatolites from the Gunflint Iron Formation (1/4). (A, B) The laminae defining the stromatolites are widely defined by the abundance of carbonaceous organic matter, which is also finely disseminated throughout the matrix, and often contain accumulations of pyrite. (C) Pyrite is also disseminated throughout the silica cements, but it is more abundant in the laminar carbonaceous patches (arrow). Note that this photomicrograph was optimized with a combination of transmitted and reflected light to show the abundance of pyrite. (D, E) Pyrite crystals often exhibit pyritohedral habits and in some cases can be zoned. (F, G) In the Schreiber locality, pyrite is often replacing the walls of ooidal features. The EDS shown in back scatter in F, was obtained in the area shown in "G". (H) Conversely, in samples from the MM location, iron oxides (arrow) occur in association with ooids cemented by microquartz.

high refractive index parallel to the crystallographic c-axis; see Fig. 5B). This is very different from primary authigenic chalcedony, which is known by exhibiting optical properties that result in a lower refractive index in the direction of the fibers; termed length-fast (Flörke et al., 1991; Graetsch, 1994; Wahl et al., 2002). In microfossiliferous stromatolites from the correlative Paleoproterozoic rocks of the Belcher Islands (central Hudson Bay, Canada) (Baragar and Scoates, 1981), this kind of cement was defined as replacive chalcedony after aragonite (Hofmann and Jackson, 1987). Similar fabrics, now composed of calcite or dolomite, are also known from numerous Phanerozoic carbonate rocks and have been interpreted as replacement products of former submarine aragonite (i.e., Davies, 1977; Mazzullo, 1980; Given and Lohmann, 1985). In this regard, Aissaoui (1985) provides details on the dissolution-precipitation processes that affect the mineralogy of Neogene examples of such fabrics.

Kerogen-rich patches that in cross-section delineate the various laminae often contain medium to coarse (60–140 µm), partially silicified, planar–e rhombohedral carbonate crystals (e.g., Fig. 5C). These carbonate cements are within a silica matrix and show corroded boundaries (Fig. 5D). When observed in SEM-EDX after an etching protocol that involved a 10-second immersion of polished samples into 6 N HCl, the partially dissolved crystals reveal intracrystalline microfabrics that suggest that they predate the pervasive silicification process (Fig. 5E). It is noteworthy that, in samples from FB within the now silica cement, we also observed displacively replaced and isolated cubic molds and mineral casts (hoppers) (Fig. 5F, G). Such textures have not been previously described for the Gunflint Formation and point to localized precipitation of halite in an evaporitic peritidal zone (e.g., Bell and Jackson, 1974).

Backscattered SEM shows that the medium- to coarsely-crystalline rhombs comprise chemically zoned crystals with a dolomitic composition and iron-rich cores (Fig. 6AB). Further 2D-XRD analyses of these rhombs show that the crystals are silicified Fe-rich members of the dolomite series, with ankeritic

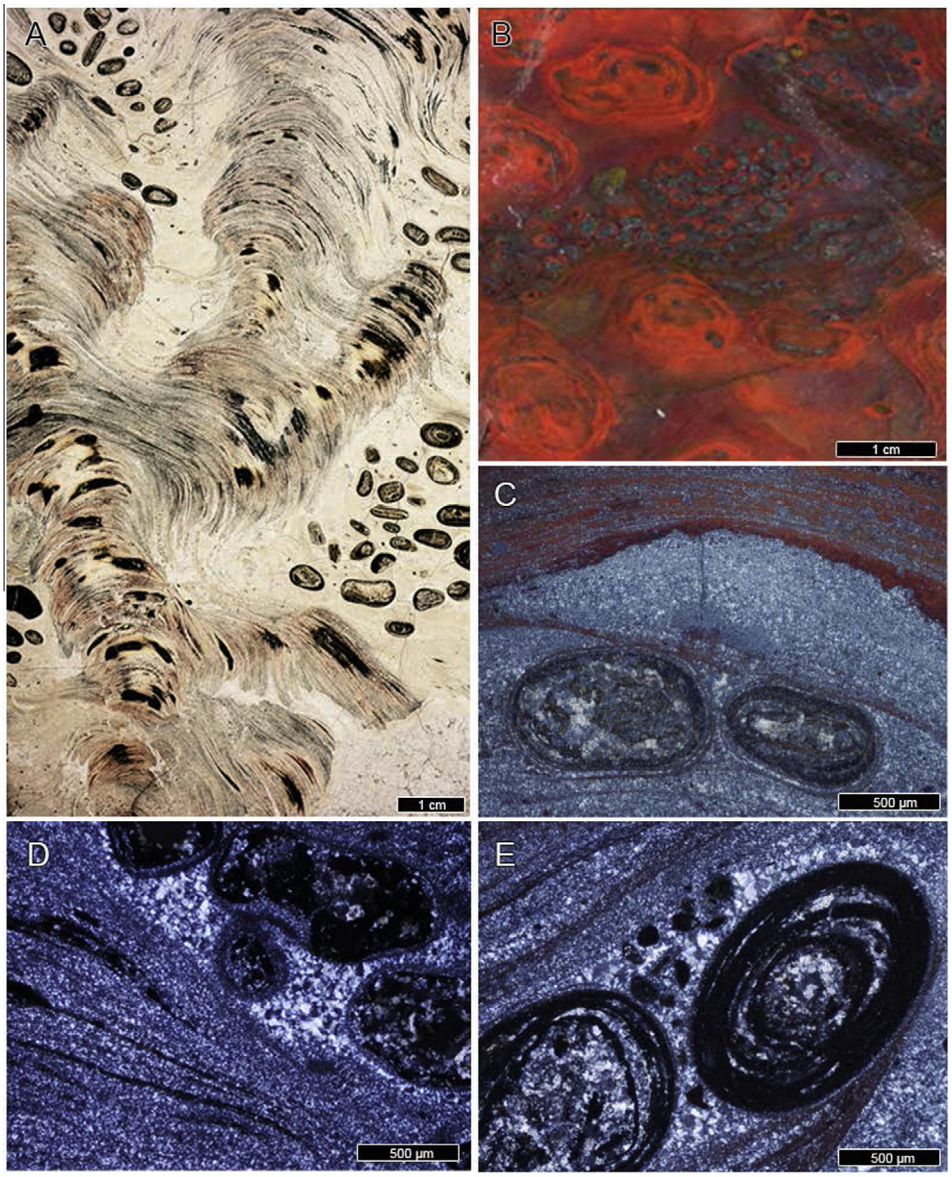

Fig. 3. Textural features of the stromatolites from the Gunflint Iron Formation (2/4). (A, B) Columnar branching multifurcate stromatolites dominate the morphotypes on the Mink Mountain locality (Upper Gunflint). (C) the stromatolitic/oolitic chert is hematite-rich. Note the abundance of coated grain infilling voids spaces among the laminar structures. (D, E) These coated grains would be intraclasts trapped at the time of stromatolite accretion, their nuclei may also be comprised of chert fragments, requiring the nuclei to have formed within reach of erosion (i.e., near the sediment-water interface). The cortical laminae are hematitic/magnetitic; the interstices are filled with drusy megaquartz.

cores and Fe-dolomite cortices (Fig. 6C, D). This petrographic observation confirms previous reports of the "Lower Algal Chert Member" near the Schreiber location, where chemically zoned euhedral carbonates interspersed within the matrix were described by Simonson and Lanier (1987) and Moreau and Sharp (2004).

Using cement fabrics as a petrographic criterion, the stromatolites from the Lower Cherty Member of the Gunflint ought to have had a primary carbonate mineralogy that precipitated in a shallow peritidal and locally evaporitic setting. This correlates well with the earlier work of Markun and Randazzo (1980) which concentrated on stromatolitic cherts from the Schreiber locality. These concordant interpretations are at odds with that of Maliva et al. (2005), who extrapolated results from granular cherts that might (or might not) be representative of ooid shoal subtidal environments, to interpret the stromatolites from the Gunflint Formation.

4.2. Geochemistry

4.2.1. Trace elements

Fig. 7 reports on the bulk rock concentrations of first row transition metals measured in Sch, FB, the hematite-bearing MM localities, and also (for comparison purposes) samples we collected from a large hemispheroid stromatolite cropping out near Kakabeka Falls (see Table 1). Vanadium was not detected in samples from Sch; measured V concentrations ([V]) in the FB reached 10.2 ± 0.7 ppm; while in the hematite-rich stromatolites from the MM, [V] are 3.3 ± 0.6 ppm. Chromium at Sch was 0.4 ± 0.1 ppm, and in the FB it reached 1.2 ± 0.3 ppm. The mean [Cr] value in MM was 17.7 ± 1.2 ppm. Iron was found in all samples analyzed; with hematitic specimens at MM averaging 3.14 ± 0.03 wt.%. In the dolomitic/ankeritic + pyritic samples, [Fe] ranges from 0.05 ± 0.01 (at Sch) to 2.02 ± 0.43 wt.% in FB stromatolites.

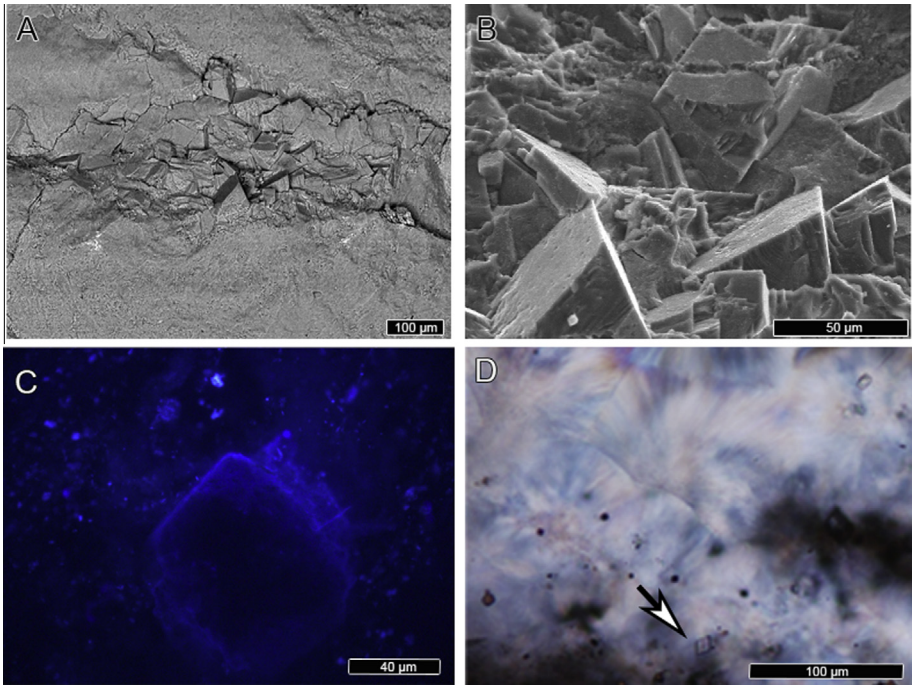

Fig. 4. Textural features of the stromatolites from the Gunflint Iron Formation (3/4). (A, B) SEM photomicrographs are showing first generation isopach cements containing microquartz and fine crystalline rhombohedral silica phases. (C) The rhombohedral features are coated by luminescent organic matter, which is also dispersed into areas dominated by microquartz, but not within the fibrous fabrics. (D) Botryoidal slow-length chalcedony occurs in a textural relation that suggests that precipitation of this cement postdate the fine-scale rhombohedral features (arrow).

Manganese was found in all of the samples, with larger contents appearing in the FB samples ([Mn] = 3177.7 ± 908.4 ppm). Samples from MM have [Mn] = 780.6 ± 157.5 ppm. The lower contents were measured in Sch ([Mn] = 34.7 ± 1.3 ppm). In Sch, [Co] and [Ni] are consistently below 1 ppm (0.6 ± 0.1 ppm). In contrast, at FB, [Co] averaged 7.1 ± 2.8 ppm and Ni was 7.0 ± 0.4 ppm. Stromatolites at the MM are relatively enriched in [Ni] (18.3 ± 0.3 ppm) but not [Co] (3.4 ± 0.5 ppm). Copper was found relatively enriched in the hematitic stromatolites of MM (9.5 ± 1.8 ppm). The stromatolites from Sch and FB have [Cu] = 4.6 ± 1.2, and 8.7 ± 6.8 ppm, respectively. Similarly, we found that Zn is relatively enriched in the hematitic stromatolites of MM (9.5 ± 1.8 ppm). By contrast, the samples from the Sch and FB have [Zn] of 2.7 ± 1.6 ppm, and 3.6 ± 1.0 ppm. In summary, the samples from MM are consistently enriched in some transition metals, with a general depletion observed in samples from the Sch.

Fig. 8 highlights a common feature in all dolomite/ankerite-bearing samples, where the distribution and abundance of some trace elements, such as Ni, Zn, and Fe, coincide with the carbonaceous laminae, and most Cu "hotspots" correspond to pyrite. The partially silicified, finely crystalline carbonate phases are reasonably homogeneous. Preferential concentrations of Mn, which does not readily form sulfides, are common in such carbonate phases. However, Mn is also predominantly found associated with kerogen/oxides-rich zones.

4.2.2. Rare earth elements

The REE systematics of ancient stromatolites has previously been used to: (1) investigate whether these elements reflect the evolving Precambrian ocean and the effects of widespread hydrothermal input (i.e., Eu anomalies, Kamber and Webb, 2001); (2) evaluate whether stromatolite accretion occurred under anoxic conditions (i.e., Ce anomalies; Van Kranendonk et al., 2003); and (3) define the environment of accretion of stromatolites (i.e., La anomalies; Bolhar and Vankranendonk, 2007; Awramik and Buchheim, 2009). In the particular case of the Gunflint Formation, only the bulk rock REE geochemistry of hematite-bearing stromatolites has been used to evaluate the paleoenvironmental redox conditions at the time of accretion (Planavsky et al., 2009). Conversely, there are no data for the REE signatures of dolomite- and pyrite-bearing stromatolites from the FB and Sch localities.

Fig. 9 shows a comparison of our REE dataset and values previously reported for stromatolites of the Gunflint Formation (i.e., Planavsky et al., 2009). Our REE concentration data are also presented in Table 2. Except for La and Eu anomalies, the shale-normalized REE patterns are smooth, which indicates excellent analytical quality (Fig. 9A). The REE_{SN} data of stromatolites of Sch show characteristically flat, slightly HREE-depleted patterns (Sch: Pr/Yb_{SN} = 1.08 ± 0.24; Pr/Sm_{SN} = 0.74 ± 0.01; and Sm/Yb_{SN} = 1.45 ± 0.29), with significant positive Eu anomalies (Eu/Eu^*_{SN} = 2.03 ± 0.40). Lanthanum displays positive anomalous values (Ce/Ce^*_{SN} = 0.83 ± 0.14), and no analytically significant Ce-anomalies (Pr/Pr^*_{SN} = 0.90 ± 0.04). The stromatolitic rocks of FB (samples FB74g, A-2-75, 1-2-75) display less marked Eu anomalies (Eu/Eu^*_{SN} = 1.34 ± 0.13) than Sch, and positive La anomalies (Ce/Ce^* = 0.87 ± 0.13), with slightly depleted HREE-patterns (Pr/Yb_{SN} = 1.61 ± 0.95; Pr/Sm_{SN} = 0.72 ± 0.04; Sm/Yb_{SN} = 1.45 ± 0.29). In both of these locations, Ce anomalies are not present (i.e., $Pr/Pr^*_{SN} \sim 1.00$) or are slightly positive (Fig. 9B). The samples from MM and Kakabeka Falls are characterized by Eu anomalous values (Eu/Eu^*_{SN} = 1.96 ± 0.15 and 1.84 + 0.36, respectively; Fig 9A) and do not display conspicuous Ce anomalies (Fig. 9B, C).

We also evaluated via μXRF the distribution of Y as an indicator of the partitioning of REE within the different solid phases comprising the dolomite-bearing stromatolites. Our interest was in determining the association of this element with Ca- and Fe-bearing phases because these are the main sinks of REE and Y in such sediments (REE+Y; Bau et al., 2014). Phosphates are also important sinks of REE (e.g., Rasmussen, 1996), yet on the stromatolitic facies of the Gunflint Formation they only occur as accessory microcrystalline apatite associated to fossilized cells (Mojzsis and Arrhenius, 1998). This in contrast with the observation of

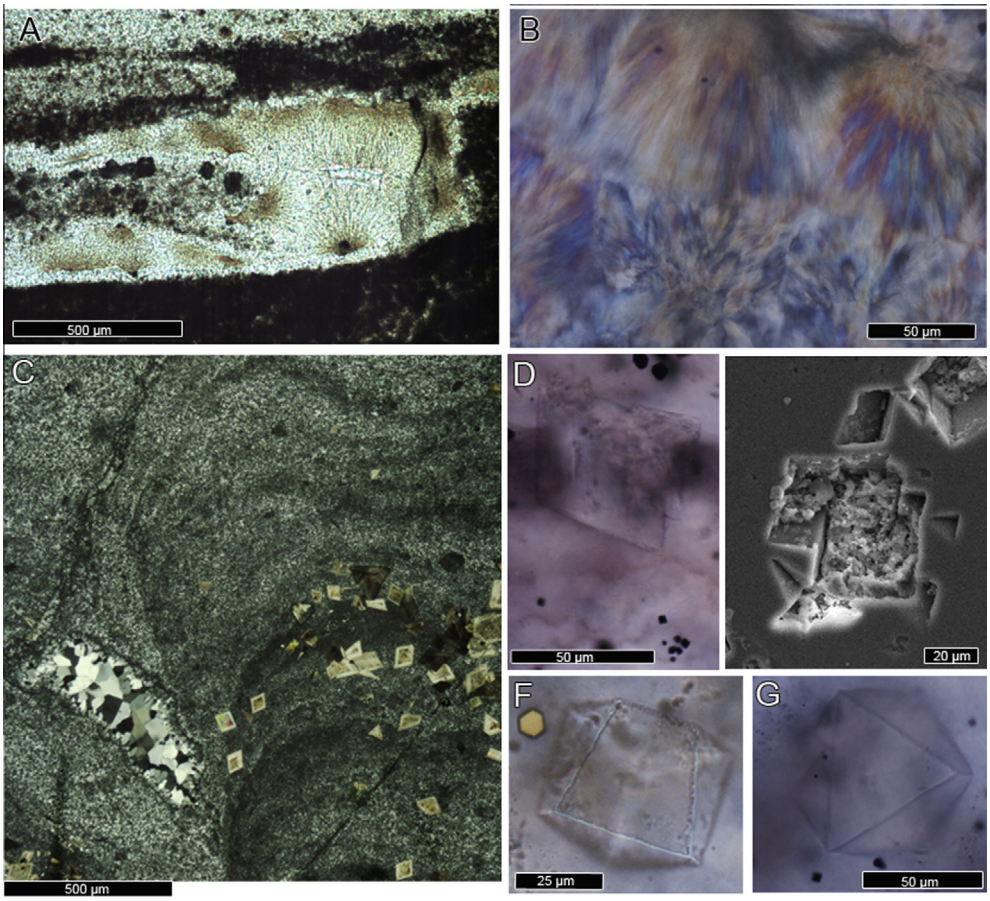

Fig. 5. Textural features of the stromatolites from the Gunflint Iron Formation (4/4). (A, B) A first generation of cement is isopachously coating both laminar and ooidal/peloidal allochems. Often a second generation of cement infilling the voids is radial-fibrous (botryoidal) chalcedony after aragonite. Notice the second order interference colors in the radiaxial cement (B: phase-contrast plus crossed nicols). (C) Detail of a small silicified branching columnar stromatolite from the Schreiber locality. Notice the local abundance of carbonate rhombs, which are restricted to the structure. This sample exhibits a pore filling drusy texture comprised of first generation isopachous quartz followed my megaquartz cement infilling void spaces. (D) Within the silica matrix on Frustration Bay samples, the silicification process preserved euhedral rhombs in apparent optical continuity with silica, these medium crystalline rhombs are often corroded. Notice pyrite crystals with different habits. (E) The kerogen-rich patches contain partially silicified planar–e rhombohedral carbonate crystals, which in polished section become much more evident after dissolution with 6 N HCl (10 s). (F, G) cubic crystal cast morphologies in a silica matrix observed in the microfossiliferous sample FB74g.

Hiatt et al. (2015) in the correlative Michigamme Formation, MI, USA, where phosphates are relatively abundant. In sample FB74g from FB, the inter-correlation diagrams obtained from individual analyses conducted in steps of ~5 µm and at an analytical area of about 500 μm^2 revealed that most Y is associated with Ca-bearing phases (Fig. 8C). Our observations shows that the finely-crystalline carbonate phases also sequestered considerable amounts of Y, which, contrary to the zonation observed in coarse multigenic phases, seem to be homogenously distributed (at least at the scale of our *in situ* µXRF analyses). The nature of fine crystalline dolomite within Ca-rich analytical areas makes it difficult to resolve the intracrystalline metal signatures of the small early formed carbonate phases preserved by the silicification of remnant microbial mats. Advances in micro-focussing technology, via sophisticated KB mirror setups, capable of reaching submicron-scale analytical areas, will permit future investigations of these phases, considered to be early diagenetic in origin (i.e., Ricketts, 1983).

5. Discussion

5.1. Mineral paragenesis on stromatolites of the Gunflint Formation

5.1.1. Petrographic and stable isotope insights

Contrary to the general model in which a viscous amorphous medium favors the growth of fibrous silica, such as silica gel (i.e., Graetsch et al., 1987), our petrographic data shows that most of the stromatolites from the Lower Gunflint Formation contain length-slow botryoidal chalcedony cement. This phase likely formed secondarily after the precipitation of fibrous carbonates (most probably aragonite). Another first generation isopachous cement appears to have been a Mg-rich carbonate, such as dolomite. As discussed above, an analogous observation was made in Paleoproterozoic stromatolites from the Belcher Islands (Hofmann and Jackson, 1987), and early formed dolomite has been also recently described in the correlative Michigamme Formation in Michigan, USA (Hiatt et al., 2015). The evidence shows that the primary carbonates precipitated subaqueously in close association with decaying organic matter, some of which was preserved as kerogen within the boundaries of rhombohedral crystals (e.g., Fig. 6C). The above interpretation is consistent with the process that would have governed the early stabilization process of these structures, which was presumably controlled by the breakdown of microbial biomass. Such microbially induced mechanisms often lead to a localized state of elevated pH and alkalinity, and thus to carbonate mineral oversaturation (see Gallagher et al., 2012).

Individual euhedral Fe-dolomite crystals locally corroded, silicified, and partially replaced by ankerite (i.e., Fig. 6) are found in the cherty matrix of the FB and Sch locations. This textural relation indicates that dolomite growth preceded precipitation of the silica as a post-depositional process (e.g., Dapples, 1979). Other

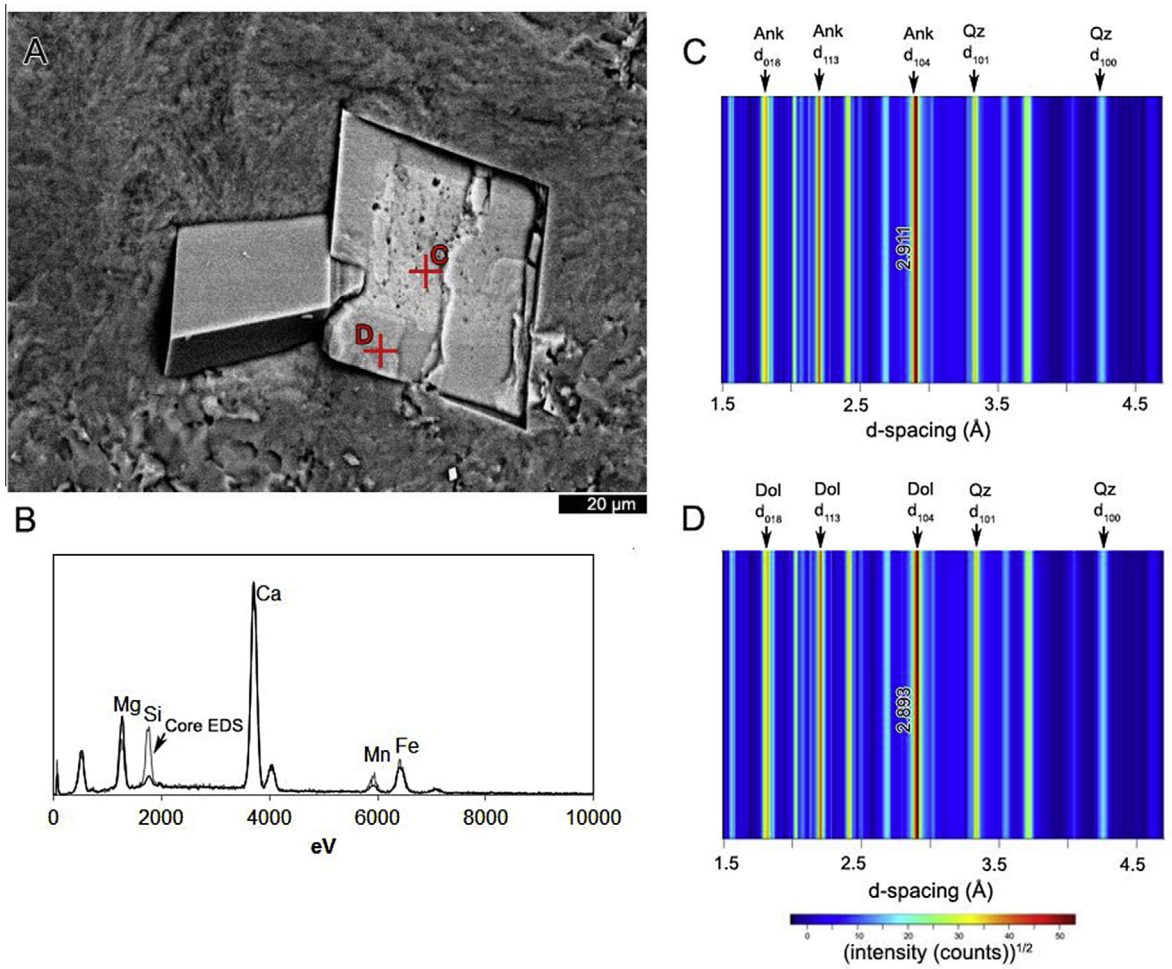

Fig. 6. Synchrotron-based XRD results on zoned carbonate from a sample from the Frustration Bay locality. (A, B) Zoned carbonate crystal (BSEM + EDS). (C, D) Fine-scale µXRD analyses of such crystals revealed that they are silicified Fe-rich members of the dolomite series, with ankeritic cores and Fe-dolomite cortices.

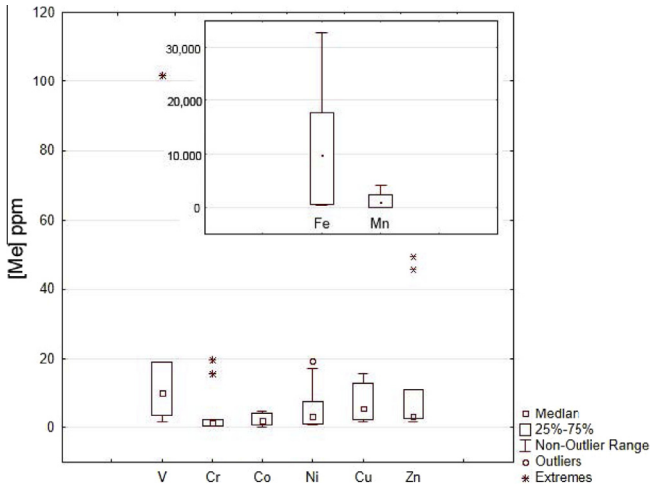

Fig. 7. Box-plot diagram is showing the concentration range of the first row transition metals ([Me]) on the stromatolite samples. The inset displays the concentration range of Fe and Mn, which are in a larger range. See further explanation in the text.

early-formed carbonate cements were completely replaced by silica due to a shallow burial silicification mechanism probably resulting from a silica oversaturated fluid permeating the structures after accretion. This early diagenetic fluid caused a coupled dissolution-precipitation reaction front, responsible for the pseudomorphic replacement of metastable carbonates. While silicification obliterated the metastable micritic and isopachous fabrics, leading to microquartz growth, it preserved the more stable rhombohedral dolomite inclusions. This is because aragonite and Mg-calcites are more soluble than dolomite under natural precipitation conditions (Morse and Mackenzie, 1990).

Replacement of primary carbonates is thought to have occurred under marine, probably evaporitic conditions, as indicated by the presence of cubic casts — interpreted here as halite — and length-slow chalcedony, which is thought to be the product of silicification of carbonate mineral phases formed under hypersaline Mg-rich conditions (Pittman and Folk, 1971; Folk and Siedlecka, 1974). Interestingly, length-slow chalcedony has been reported in other petrographic studies of the Lower Cherty Member (i.e., Markun and Randazzo, 1980), but was notably absent in oolitic chert microfacies studied by Maliva et al. (2005). Sommers et al. (2000) also provided evidence pointing to a secondary silica replacement of primary carbonate ooids in rocks from the microfossiliferous Whitefish Falls locality in Nolalu, Ontario.

A general geochemical and thermodynamic requirement for silicification of carbonates is the existence of pore fluids supersaturated with respect to silica, and undersaturated with respect to the carbonate mineral that becomes dissolved (Hesse, 1989). Reported mechanisms for replacement of carbonates by silica are: (1) microbial metabolisms capable of locally lowering the pH, thus affecting metastable carbonate solubility and inducing

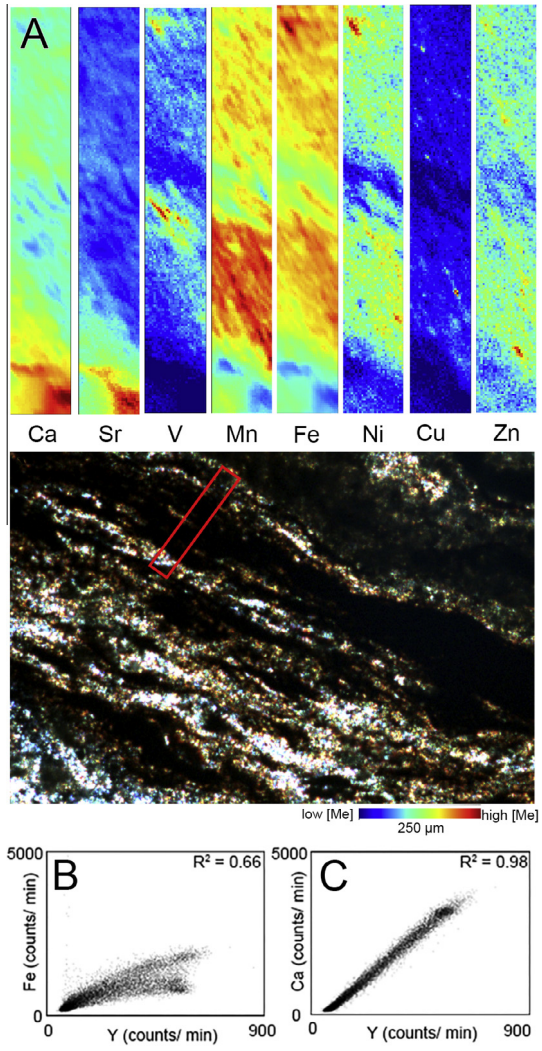

Fig. 8. Micro-XRF elemental maps. The panels show a representative laminar zone of a stromatolite from the Frustration Bay microfossiliferous locality of the Gunflint Formation (sample is FB74g). The color-coding convention assigns blue to the minimum and red to maximum deconvoluted peak area of the element. (B, C) Elemental correlation plots, they show that most Y (and probably HREE, see main text) is associated with Ca-bearing phases. Note that an important fraction of Fe is within Fe-Ca carbonates (i.e., ankerite and ferroan dolomite). (For interpretation of the references to color in this figure legend, the reader is referred to the web version of this article.)

silica precipitation (see Siever, 1962; Knoll, 1985; Clayton, 1986) and/or (2) the mixing of marine and continental waters, which can also induce a decrease in pore water pH (Knauth, 1979). The silicification process not only resulted in the fossilization of microbial cells beneath the surface, but also allowed for crystallographic orientations to be inherited from parent carbonate to product silica. Fluctuations in pH around the circumneutral and alkaline range in a hypersaline setting are thus considered crucial controlling factors for such silicification processes.

As proposed by Simonson and Hassler (1996), pervasive silicification was completed during shallow burial diagenesis, likely prompted by shifts in base sea level, which allowed for the mixing of marine and continental waters. By locally affecting the chemistry of peritidal environments, such mixing process would have also shifted the saturation states of iron-bearing minerals, leading to replacement of the metastable dolomite cores by ankerite; while the less soluble Fe-dolomite crystal cortices prevailed (e.g., see Jones, 2013). In this regard, the multiple growth stages observed in pyrite suggest the partial oxidation of this phase as a likely mechanism for ankerite oversaturation of the internal precipitation environment within the stromatolites. Although some other iron-bearing minerals have been considered primary in origin (i.e., Planavsky et al., 2009), a more detailed study recently suggested instead that siderite might very well be a secondary carbonate mineral (Shapiro and Konhauser, 2015). Regarding hematite, these authors also pointed out that this mineral only dominates in areas where stromatolite-bearing horizons are in contact with Mesoproterozoic diabase sills and dikes of the Duluth Complex.

The abundance of siderite within hematitic stromatolite microfacies contrasts with its lack in ankerite/dolomite-bearing stromatolites and points to laterally variable paleoenvironmental chemistry and post-depositional diagenesis. These mineralogically dissimilar stromatolites, however, exhibit strikingly similar morphotypes, which suggests that these sedimentary structures represent a comparable accretionary setting but dissimilar diagenetic subenvironments. An early siderite phase would have formed from the enrichment in pore-water Fe(II) via subsurface Fe(III)-reducing microbes (Konhauser et al., 2005; Fischer et al., 2009), thus allowing Fe(II) to be in excess of biologically produced HS^-. Under this condition, Fe(II) was removed from solution in the presence of bicarbonate, leading to the formation of siderite (e.g., Coleman, 1985; Curtis et al., 1986). It should be recalled, however, that in the presence of moderate concentrations of sulfate, such as those characterizing most Paleoproterozoic continental margins (Partin et al., 2015), siderite precipitation promoted by Fe(III) reduction would be followed by the alteration of siderite to pyrite by sulfate reducers (e.g., Kenward et al., 2009). In this regard, *in situ* analyses of pyritized microfossils in stromatolites from the Schreiber locality suggest that these structures were stabilized in a diagenetic realm where the activity of sulfate reducers had initial significance, but were progressively limited by porosity occlusion linked to silica oversaturation and precipitation (Wacey et al., 2013). Our petrographic analyses of the FB and Sch samples further indicate that as silicification occurred, the early formed dolomite was preserved, but most, if not all, early formed siderite was dissolved.

Interestingly, as opposed to hematite that was previously reported in samples from the Schreiber Beach (Planavsky et al., 2009), our samples from this locality not only lack this phase, but the walls of some of the ooids are instead replaced by pyrite. Papineau et al. (2005) also report pyrite in cherts from Sch and measured their sulfur isotope signatures. Their study revealed a small range of $\delta^{34}S$ values (CDT) between +1.09 and +0.42‰ and $\Delta^{33}S$ values between +0.02 and +0.15‰. This range of values, however, does not allow for the identification of the sulfur source or inference on the oxygenation conditions at the time of precipitation (Papineau et al., 2005). At the correlative FB locality we observed that the majority of small pyrite grains occurred within kerogen-rich laminar areas (Fig. 5B, D). This could mean that either pyrite precipitated in association with the degradation of stromatolite-building microbial mats, or that it represents trapped crystals from desegregated framboids transported to the shallow shelf contemporaneous to stromatolite accretion. Based on textural evidence, and incorporating models that invoke a chemically stratified Animikie Basin (Poulton et al., 2004, 2010), an alternative mechanism for the localized abundance of pyrite is possible: transport of fine-grained pyrite precipitated in the water column to the shallow-marine loci of stromatolite accretion. Such a mechanism has been found capable of drawing pyrite in suspension from anoxic/euxinic deep redoxclines onto the shallow shelf, leading to the deposition of disaggregated framboids (see Kershaw et al., 2012; Kershaw, 2015).

Based on textural analyses, we propose that fluids undersaturated with respect to dolomite led to the partial dissolution of dolomite cores, and the precipitation of silicified ankerite may be

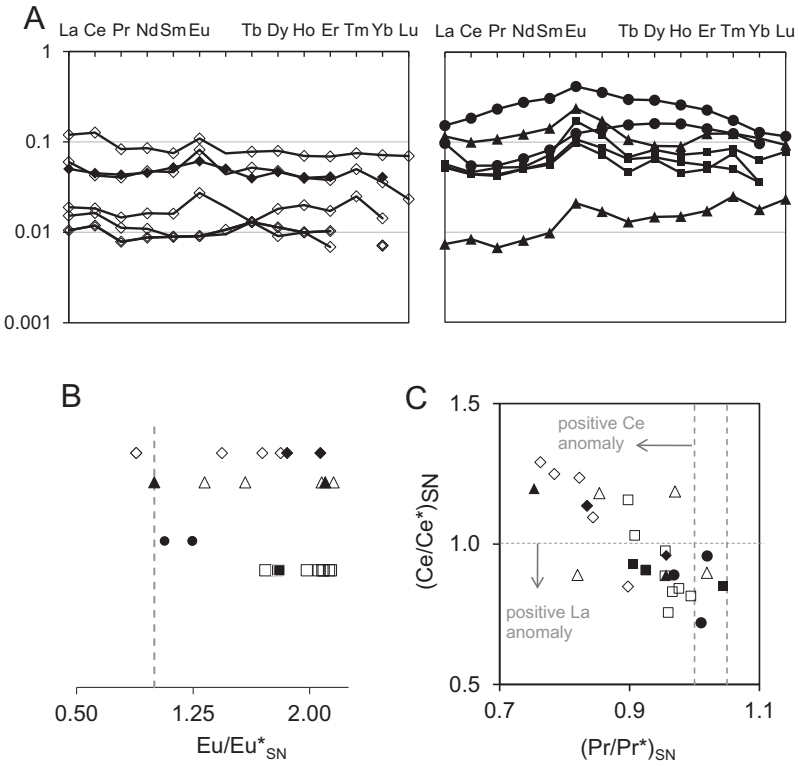

Fig. 9. Shale-normalized REE diagrams (Post-Archean Australian Shale (PAAS) values of Taylor and McLennan (1985)). (A) Spider plots comparing values from representative non–hematitic and hematic stromatolites. (B, C) Diagrams after Bau and Dulski (1996). Filled data points are data from this study; unfilled data points from Planavsky et al. (2009).

Table 2
REE data (ppm) pertaining the studied stromatolites.

Sample name and locality	La	Ce	Pr	Nd	Sm	Eu	Gd	Tb	Dy	Ho	Er	Tm	Yb	Lu
Frustration Bay (FB)														
FB74g1	6.51	17.17	2.56	11.21	2.24	0.60		0.26	1.37	0.27	0.65	0.06	0.33	0.04
FB74g1	5.82	14.82	2.08	8.89	1.72	0.46		0.23	1.29	0.26	0.66	0.07	0.36	0.05
A.2-75	3.69	4.38	0.49	2.10	0.46	0.14		0.12	0.71	0.16	0.41	0.05	0.27	<DL
Schreiber (Sch)														
Sch 1-2-1	2.03	3.53	0.39	1.62	0.33	0.12		0.05	0.30	0.06	0.16	0.02	0.10	<DL
Sch 1-2-2	1.98	3.52	0.38	1.61	0.32	0.11		0.04	0.29	0.05	0.15	0.03	0.10	<DL
Sch 1-4-1	2.17	3.70	0.46	1.69	0.40	0.19		0.05	0.36	0.07	0.22	0.03	0.18	0.03
Mink Mountain (MM)														
MkM3	1.91	3.61	0.39	1.46	0.26	0.10		0.03	0.21	0.04	0.12	<DL	0.11	<DL
MkM4	0.65	1.39	0.12	0.44	0.10	0.05		0.04	0.22	0.03	<DL	0.03	<DL	<DL
Kakabeka Falls														
Kaf 2-1	4.41	8.01	0.97	3.93	0.80	0.31		0.09	0.50	0.12	0.36	0.05	0.31	0.04
Kaf 2-2	0.28	0.67	0.06	0.26	0.06	0.02		0.01	0.07	0.02	0.05	0.01	0.01	0.01

associated with the diagenetic solubilization of iron from pyrite within the structures. The presence of disseminated chemically zoned-pyrite in specimens from FB suggests multiple post-depositional stages of pyrite dissolution and growth probably caused by repeated cycles of subaerial exposure and intertidal submergence. The ankerite cores precipitated inside hollow crystals that produced inside-out ankerite crystals that have an ankerite core encased by a Fe-dolomite cortex. The Fe-dolomite overgrowths may have precipitated under the influence of methanogenic and Fe(III) reducing bacterial communities operating in a near-surface diagenetic environment (e.g., Coleman, 1985; Curtis et al., 1986; Konhauser et al., 2005; Beal et al., 2009), but *in situ* carbonate $\delta^{13}C$ analyses would be required to test this hypothesis. Variations in pH linked to pyrite solubilisation would have caused dissolution of primary Ca-rich dolomite in the cores of the crystals (see Jones, 2013, and references therein), which latter — in a HS^- limited, but alkaline re-precipitation environment — resulted in the co-precipitation of iron and manganese into the core-replacive ankerite phase. As observed by Marin et al. (2010), the petrographic evidence indicates that this process predates microquartz and megaquartz formation and occurs under silica-saturated pore water conditions. Recent nanoscale isotope analyses of pyritized microfossils in samples from the Sch location (Wacey et al., 2013), reveals that owing to coeval silicification, sulfate anion concentrations became rapidly depleted leading to dispersion of the sulfur isotope signature. Such a result places additional constrains on the timing of precipitation of the mineral assemblage.

Bulk rock measurements of $\delta^{13}C$ in carbonates from stromatolitic cherts of the Lower Gunflint also offer some insight, but their interpretation is not straightforward. Previous work has shown

that they average −2.9‰ (Strauss and Moore, 1992), and in the microfossiliferous chert outcropping at the Frustration Bay locality, they exhibit near 0‰ values (Winter and Knauth, 1992). This $\delta^{13}C$ signature is also observed in early formed ankerite and siderite phases comprising analog facies of the Upper Gunflint, and has been interpreted as the result of a dominant marine bicarbonate source during carbonate mineral stabilization (e.g., Carrigan and Cameron, 1991). When this presumably seawater-derived signature ($\delta^{13}C \approx 0‰$) is contrasted with the *in situ* organic carbon isotope content of *bona fide* Gunflint microfossils (−32 to −45‰; House et al., 2000), the organic $\delta^{13}C$ values seem too negative to be attributed to isotopic fractionation by cyanobacteria, and generally too positive to be attributed to isotopic fractionation by methanogens (Wacey et al., 2011). Nevertheless, elevated pCO_2 levels and hence high dissolved CO_2 concentrations in the surface Paleoproterozoic ocean (Sheldon, 2006) should have been concomitant with increased biological discrimination against ^{13}C during neritic microbial photosynthesis (see Hollander and McKenzie, 1991; also Riding, 2006). It is also the case that variations in the $\delta^{13}C$ values of marine organic matter can only be temporarily mirrored by the ^{13}C values of seawater DIC (e.g., Naafs et al., 2016). Therefore, not only would the $\delta^{13}C \approx 0‰$ of carbonates in the Gunflint Formation point directly to a predominant marine bicarbonate source during carbonate mineral stabilization, but the biological fractionation discussed by Wacey et al. (2011) is likely linked to redox stratification concurrent with fluctuations in the DIC and DOC reservoirs in the Precambrian ocean (i.e., Bekker et al., 2008; Poulton et al., 2010).

Incidentally, in the Upper Gunflint member the $\delta^{13}C$ values of second generation carbonates are shifted toward lighter values (down to −7‰), suggesting a more significant incorporation of oxidized organic carbon during diagenesis (Carrigan and Cameron, 1991). The ^{13}C contents of such Fe-rich carbonate phases, however, contrast with the isotopic carbon signature that could be expected for Fe(III) reduction ($\delta^{13}C \approx -25$ to −10‰; Coleman and Raiswell, 1993). As such, it was argued that the bulk rock carbon isotope data of the unmetamorphosed carbonates of the Gunflint Formation reflect the combined effect of a variable admixture of DIC influenced by microbial Fe(III) reduction (e.g., Bekker et al., 2010) and sulfate reduction (e.g., Wacey et al., 2013), with seawater bicarbonate and DIC evolved during shallow burial methanogenesis (e.g., Carrigan and Cameron, 1991). Bearing in mind that silicification likely minimized pore-water flow and hence closed these isotope systems early during diagenesis (Wacey et al., 2013), then a careful evaluation of the multi-isotope signals of carbonates in the stromatolites of the Gunflint Formation would offer insight into the problems in using carbon isotope signatures to recognize specific microbial processes (see Raiswell and Fisher, 2000 for details) and the apparent decoupling of the Paleoproterozoic carbonate and organic carbon records (Bekker et al., 2008). Probing such signatures in the range of carbonate mineralogies discussed here still presents an instrumental difficulty (see Riciputi et al., 1998 for details).

Overall, our petrographic insights and the evaluation of reported stable isotopes data allow us to propose the following mineralization sequence for the stromatolites of the Gunflint Formation:

1. Mg-calcite, aragonite, and minor dolomite co-precipitated subaqueously, infilling the void spaces of the organo-sedimentary structures. Their precipitation was linked to the degradation of labile organic matter of microbial origin, which may also have led to some primary pyrite precipitation. This was probably concomitant with early formed siderite dissolution followed by authigenic pyrite precipitation. Locally, halite co-precipitated with carbonates.
2. Early diagenetic replacement of metastable carbonate cements and halite by silica, with minor early formed dolomite crystals preserved.
3. Partial dissolution of primary dolomite in association with pyrite oxidation, followed by Fe-dolomite overgrowth and replacement of early formed dolomite cores by ankerite. The ankerite precipitated prior to the onset of megaquartz formation infilling the remaining void space of the stromatolitic structures (cf. Marin et al., 2010).
4. In areas affected by Fe-rich pore waters that evolved after a Mesoproterozoic mafic intrusion (Shapiro and Konhauser, 2015), oxidation of Fe(II) first decreased the pH of the pore water system, and thus led to complete dissolution of both first and second generation carbonates, with subsequent precipitation, on a regional basis, of hematite (in the presence of pore-water O_2). As conditions favourable for Fe(III) reduction were progressively reinstated, a second stage of alkalinity production, with low biologically produced HS^-, allow for siderite precipitation (in the absence of pore-water O_2). There was also additional silicification.

5.1.2. Other geochemical insights

The various samples analyzed show insignificant (i.e., $Ce/Ce^* \sim 1.0$) to positive La anomalies (mean: 0.95, median: 0.93). Variability in these anomalies between sites would have resulted from lateral variation in marine vs. continental influences in the peritidal realm, with areas affected by runoff probably exhibiting dilution of a seawater-derived La signature; although positive La anomalies might not be limited to marine settings (e.g., Johannesson et al., 2006, their Fig. 9).

Europium anomalies were not detected in our samples from the Sch, but are present in samples from the FB and MM, probably reflecting the local effects of exhalative hydrothermal input over the post-depositional redistribution of REE in both the Lower Cherty Member (i.e., FB) and the Upper Cherty Member (i.e., MM). Post-depositional alteration would have locally affected the primary REE contents and altered the initial Eu anomalies (Shields and Stille, 2001).

Siderite + hematite-bearing samples display REE series and Ce-anomalies (Pr/Pr^*) patterns that are essentially similar to those of the samples composed of dolomite/ankerite + pyrite (Fig. 9A). Under the dissimilar physicochemical conditions controlling the precipitation of these purportedly primary mineral assemblages, the REE should have exhibited fundamentally different complexation behavior, reflecting aqueous and mineral-specific REE fractionation during incorporation into their respective early diagenetic phase. This, in turn, should have produced dissimilar REE abundances and distribution trends (Kawabe et al., 1999; Bau and Koschinsky, 2009). For instance, in modern seawater, primary carbonate minerals exhibit a preferential scavenging of light REE compared to heavy REE when compared to primary hydroxide minerals (Elderfield, 1988; De Baar et al., 1988, 1991). Accordingly, the REE_{SN} patterns of Fe–oxide minerals should display different shale-normalized ratios and distribution patterns when compared with carbonate minerals (Bau and Dulski, 1996; Bau et al., 2014), particularly if both of them precipitated from a Paleoproterozoic seawater source. Thus, our results suggest that bulk shale-normalized REE values of the Lower Gunflint stromatolites could not be a pristine record of the redox conditions prevailing at the time of early microbial mat mineralization.

By following the same line of thinking, and considering as well the dissimilar redox conditions that would have characterized the accretionary environments of our samples, then their similar anomalous bulk shale-normalized Pr/Pr^* values represents an suspicious feature. This feature cannot be discriminated by using the stromatolite mineral assemblage as a criterion. Our combined

dataset suggests that the mineral association siderite + hematite results from a ferruginous mineral stabilization environment probably influenced by exposure of Fe(II)-bearing exogenous fluids to rising atmospheric oxygen levels, and little to none biologically produced HS^-. As suggested by Shapiro and Konhauser (2015), this mineral association would have resulted from a post-depositional mixing process involving the localized Mesoproterozoic flow of reducing exogenous fluids trough the stromatolititic horizons now comprising the Upper Gunflint Formation. Hence, hematite precipitated when the Fe(II)-bearing pore water system came into contact with oxidizing meteoric fluids percolating the sequence; while siderite precipitated after Fe(II) reduction, when this pore water system affected by meteoric water admixture became alkaline and O_2 depleted (Shapiro and Konhauser, 2015).

On the other hand, and as discussed above, the dolomite/ankerite + pyrite bearing stromatolites could be considered a better-preserved early diagenetic precipitation environment, where the marine ferruginous conditions that interacted with biologically produced HS^- prior to silicification (Wacey et al., 2013), were not largely affected by the admixture process described above. Given that Ce is the only REE relevant for redox interpretations, our results suggest that bulk shale-normalized REEs values of the Gunflint stromatolites indicate that the redox conditions prevailing at the time of early microbial mat mineralization were not responsible of the localized abundance of hematite.

By comparing the REE_{SN} signatures of carbonate- and pyrite-bearing stromatolites with those of their hematite- and siderite-bearing analogues, our bulk data reveal that rather than supporting a redox stratified shallow water column, the trace element inventories of these stromatolites reflect a dissimilar burial diagenetic history. Therefore, the textural features and chemical signals of stromatolite facies in the Gunflint Formation more likely reflect contrasting rates of continental runoff and solute delivery, or the temporarily and spatially variable evolution of diagenetic fluids due to mixing with exogenous fluids, rather than the vertical redox structure of shallow Precambrian seas.

5.2. Perspectives

By the late Archean and during the Paleoproterozoic, the range of early diagenetic reactions leading to marine authigenesis in ancient peritidal settings were increasingly influenced by inputs of oxidative weathering products, such as increasing fluxes of sulfate and trace metals (Konhauser et al., 2011). The fluxes were, in turn, controlled by various cyclic depositional controls, such as relative sea-level and climate changes (Eriksson et al., 1998; Sommers et al., 2000), that were capable of drastically affecting the chemical composition of pore-waters and the minerals precipitated in equilibrium with those waters. Hydrothermal fluids may have also been locally important for diagenetic mineral stabilization (see Walter, 1972; Stille and Clauer, 1986; Sommers and Awramik, 1996).

The detailed characterization of the style and extent of diagenetic alteration is a critical first step in evaluating the primary composition of ancient stromatolites, and hence the chemistry of the solutions once in equilibrium with the mineral comprising the accreting stromatolite structures (cf. Dickson, 2009). In this regard, similarities and/or differences between the REE distribution of these structures cannot solely be explained by the REE speciation in seawater, as the reactive solid phases originally stabilizing within the stromatolites had different scavenging properties (see Bau and Koschinsky, 2009). Moreover, because they were trapped, bound or precipitated within microbial mats, the REE content would have been progressively remobilized and incorporated into secondary phases only after the breakdown of the organometallic bonds and the reduction of the ferric oxyhydroxides took place. The remobilization of metals of interest is variable and proportional to the rates of disincorporation of these elements into their primary binding phase; while the rates of incorporation into secondary phases was not only a function of the preferential affinity of these metals for the available organic ligands, but also of the variable physicochemical conditions governing the diagenetic alteration process within the structures (e.g., Petrash et al., 2012). Regarding REE, recent work by Johannesson et al. (2014) found a strong pH dependence of REE uptake by modern microbialites, which results from significant changes in La speciation in the circumneutral pH range. All of these factors can be further complicated by the fact that shallow burial diagenetic mixing of marine-derived and exogenous waters can also lead to elemental mobilization and partitioning (Shields and Stille, 2001).

From the discussion above we conclude that bulk rock datasets of Paleoproterozoic stromatolites do not permit unequivocal predictions on how the diagenetic fluids and silicifying solutions that were once in equilibrium with contemporaneous seawater interacted with the microbialite-constructing communities responsible for the "algal" (stromatolitic) facies, or how they affected the primary bulk-rock chemical signals. These fluids interacted with the microbialite-constructing communities responsible for the "algal" (stromatolitic) facies, such as those interrogated in the Gunflint Formation, where the preservation of a primary bulk-rock chemical signal seems unlikely. Clearly, more investigation of metal uptake by lithifying biological systems is necessary to evaluate whether or not the multigenic mineral assemblages comprising ancient stromatolites would have recorded a seawater-derived signature vs. the temporally and spatially variable diagenetic fluids that influenced their multi-step precipitation process (cf., Johannesson et al., 2014). In this regard, laboratory experiments (e.g., Robbins et al., 2015; Picard et al., 2015) offer an attractive avenue for further assessing the extent of preservation of primary transition metals and REE partition patterns under diagenetic conditions.

Furthermore, *in situ* analyses of chemical zoning of carbonates within the studied stromatolites using microprobes with high spatial resolution and sensitivity would be useful to clarify the early diagenetic picture that emerges from our re-assessment. These may offer an accurate record of progressive changes in the diagenetic redox conditions during crystal growth, but in most cases, their values are far from being a record of the concentration values of redox-sensitive elements in seawater at the time of precipitation. In this regard, only fine crystalline and well-preserved carbonates, such as those described here, or as detailed by Lepot et al. (2008) in stromatolites from Tumbiana Formation in Western Australia, are appropriate for use in the determination of paleo-seawater composition. Nonetheless, the small crystal size of such early formed crystals represents an analytical challenge that can only be undertaken by applying emerging micro- and nano-focused methods and accurate instrumental calibration protocols.

6. Conclusions

Validating the model of stratification of Precambrian oceans requires detailed information on the redox-sensitive trace metal concentrations of Precambrian shallow marine rocks. Such successions are of paramount importance to resolving the spatial variability in ancient oceanic redox structure. Difficulties surrounding the application of bulk-rock chemical indicators to interpret the depositional conditions of peritidal facies include: (1) uncertainties on whether the elemental systematics of authigenic minerals comprising these structures reflect early biological vs. secondary abiological processes; (2) difficulties in elucidating the primary origin of specific elemental signatures of silica phases,

some of which might be pseudomorphs after primary carbonates; (3) the general lack of understanding on how diverse syn- and post-depositional processes, that are dependent on poorly known sea level, burial, and exhumation histories, would have shifted the primary signatures of the early formed precipitates; and (4) variable circulations patterns and exogenous sources of elements, which may have also been responsible for significant post-depositional mineralogical variations.

Our data, taken together with the stratabound relation described by Shapiro and Konhauser (2015), show that the abundance of hematite and siderite within the Gunflint stromatolites might well represent a localized burial diagenetic condition. Were these minerals primary in origin as generally accepted (i.e., after Floran and Papike, 1978), then the similitude of the bulk rock REE signatures of the stromatolite samples evaluated here suggests that shale-normalized Ce anomalies of these structures might not be amenable for regional scales redox paleoceanographic interpretations. In view of our results, interpretations of shallow marine redox stratification by solely using parameters such as Ce anomalies and poorly constrained isotope systems are not valid.

Should *in situ* transition metal signatures and REE data of stromatolites be used in further paleoenvironmental investigations, recrystallized carbonate phases must be avoided for interpretations of paleo-seawater composition. Perhaps the small size primary dolomite crystals described here offer such an opportunity. However, the presence of kerogen and other inclusions together with the relatively low spatial resolution of currently available laser ablation techniques (e.g., 45 μm in diameter or above) make it difficult to target such primary phases. A more extended use of rapidly advancing photon and ion probes with a sub-micrometer scale resolution could provide a solution to this analytical challenge.

Acknowledgments

Samples from the Frustration Bay locality were provided by Stanley Awramik. Dominic Papineau is thanked for critically reviewing an early version of this manuscript and for valuable discussions. We thank Karen Johannesson and an anonymous reviewer of *Precambrian Geology* for constructive criticism and suggestions that considerably improved the final manuscript. We also thank Randall Parrish for editorial handling. Support for this work was provided by the Natural Sciences and Engineering Research Council of Canada (NSERC) to K.O.K., and National Science Foundation (NSF) to R.S.S. and S.J.M. L.J.R. gratefully acknowledges the support of a Vanier Canada Graduate Scholarship. The expertise of Robert Gordon (CLS@APS) was critical for successful analyses at beamline 20ID at the Advanced Photon Source (APS). Use of the APS, an Office of Science User Facility operated for the U.S. Department of Energy (DOE) Office of Science by Argonne National Laboratory, was supported by the U.S. DOE under Contract No. DE-AC02-06CH11357. Guangcheng Chen at the UofA Radio Isotope Facility is thanked for his assistance with ICP-MS analyses.

References

Aissaoui, D.M., 1985. Botryoidal aragonite and its diagenesis. Sedimentology 32, 345–361.
Awramik, S.M., Buchheim, H.P., 2009. A giant, Late Archean lake system: the Meentheena Member (Tumbiana Formation; Fortescue Group), Western Australia. Precambrian Res. 174, 215–240.
Awramik, S.M., Barghoorn, E.S., 1977. The Gunflint Microbiota. Precambrian Res. 5, 121–142.
Baragar, W., Scoates, F., 1981. The Circum-Superior belt: a Proterozoic plate margin? In: Kröner, A. (Ed.), Precambrian Plate Tectonics. Elsevier, Amsterdam, pp. 295–330.
Barghoorn, E.S., Tyler, S.A., 1965. Microorganisms from the Gunflint Chert. Science 147, 563–575.
Bau, M., Dulski, P., 1996. Distribution of yttrium and rare-earth elements in the Penge and Kuruman iron-formations, Transvaal Supergroup, South Africa. Precambrian Res. 79, 37–55.
Bau, M., Koschinsky, A., 2009. Oxidative scavenging of cerium on hydrous Fe oxide: evidence from the distribution of rare earth elements and yttrium between Fe oxides and Mn oxides in hydrogenetic ferromanganese crusts. Geochem. J. 43, 37–47.
Bau, M., Möller, P., 1993. Rare earth element systematics of the chemically precipitated component in Early Precambrian iron formations and the evolution of the terrestrial atmosphere-hydrosphere-lithosphere system. Geochim. Cosmochim. Acta 57 (10), 2239–2249.
Bau, M., Schmidt, K., Koschinsky, A., Hein, J., Kuhn, T., Usui, A., 2014. Discriminating between different genetic types of marine ferro-manganese crusts and nodules based on rare earth elements and yttrium. Chem. Geol. 381, 1–9.
Beal, E.J., House, C.H., Orphan, V.J., 2009. Manganese- and iron-dependent marine methane oxidation. Science 325, 184–187.
Bekker, A., Holmden, C., Beukes, N.J., Kenig, F., Eglingtone, B., Patterson, W.P., 2008. Fractionation between inorganic and organic carbon during the Lomagundi (2.22-2.1 Ga) carbon isotope excursion. Earth Planet. Sci. Lett. 271, 278–291.
Bekker, A., Slack, J., Planavsky, N., Krapez, B., Hofmann, A., Konhauser, K.O., Rouxel, O.J., 2010. Iron formation: the sedimentary product of a complex interplay among mantle, tectonic, oceanic, and biospheric processes. Econ. Geol. 105, 467–508.
Bell, R., Jackson, G., 1974. Aphebian halite and sulphate indications in the Belcher Group, Northwest Territories. Can. J. Earth Sci. 11, 722–728.
Bolhar, R., Vankranendonk, M., 2007. A non-marine depositional setting for the northern Fortescue Group, Pilbara Craton, inferred from trace element geochemistry of stromatolitic carbonates. Precambrian Res. 155, 229–250.
Bolhar, R., Kamber, B.S., Moorbath, S., Fedo, C.M., Whitehouse, M.J., 2004. Characterization of early Archean chemical sediments by trace element signatures. Earth Planet. Sci. Lett. 222 (1), 43–60.
Broderick, T.M., 1920. Economic geology and stratigraphy of the Gunflint iron district, Minnesota. Econ. Geol. 15, 422–452.
Buick, R., Dunlop, J.S.R., 1990. Evaporitic sediments of Early Archean age from the Warrawoona Group, Western Australia. Sedimentology 37, 247–278.
Carrigan, W.J., Cameron, E.M., 1991. Petrological and stable isotope studies of carbonate and sulfide minerals from the Gunflint Formation, Ontario: evidence for the origin of early Proterozoic iron-formation. Precambrian Res. 52, 347–380.
Cheatham, M.M., Sangrey, W.F., White, W.M., 1993. Sources of error in external calibration ICPMS analysis of geological samples and an improved non-linear drift correction procedure. Spectrochim. Acta 48B, E487-506.
Clayton, C.J., 1986. The chemical environment of flint formation in Upper Cretaceous chalks. In: Sieveking, G., de, G., Hart, M.B. (Eds.), The Scientific Study of Flint and Chert. Cambridge University Press, Cambridge, pp. 43–54.
Cloud, P., 1965. Significance of the Gunflint (Precambrian) flora. Science 148, 27–35.
Coleman, M.L., 1985. Geochemistry of diagenetic non-silicate minerals, Kinetic considerations. Philos. Trans. R. Soc. London 315, 39–56.
Coleman, M.L., Raiswell, R., 1993. Microbial mineralization of organic matter: mechanisms of self-organization and inferred rates of precipitation of diagenetic minerals. Philos. Trans. R. Soc. A: Math., Phys. Eng. Sci. 344, 69–87.
Curtis, C.D., Coleman, M.L., Love, L.G., 1986. Porewater evolution during sediment burial fromisotopic andmineral chemistry of calcite, dolomite and siderite concretions. Geochim. Cosmochim. Acta 50, 2321–2334.
Dapples, E.C., 1979. Silica as an agent in diagenesis in Diagenesis. In: Larsen, G., Chilingar, G.V. (Eds.), Diagenesis in Sediments and Sedimentary Rocks. Developments in Sedimentology 25A. Elsevier, pp. 99–141.
Davies, G.R., 1977. Former magnesian calcite and aragonite submarine cements in upper Paleozoic reefs of the Canadian arctic: a summary. Geology 5, 11–15.
De Baar, H.J.W., German, C.R., Elderfield, H., van Gaans, P., 1988. Rare earth element distributions in anoxic waters of the Cariaco Trench. Geochim. Cosmochim. Acta 52, 1203–1219.
De Baar, H.J.W., Schijf, J., Byrne, R.H., 1991. Solution chemistry of the rare earth elements in seawater. Eur. J. Solid State Inorg. Chem. 28, 357–373.
Derry, L.A., Jacobsen, S.B., 1990. The chemical evolution of Precambrian seawater: evidence from REEs in banded iron formations. Geochim. Cosmochim. Acta 54 (11), 2965–2977.
Dickson, J.A.D., 2009. Mississippian Paleocean Chemistry from Biotic and Abiotic Carbonate, Muleshoe Mound, Lake Valley Formation, New Mexico, U.S.A. – Discussion. J. Sediment. Res. 79, 42–43.
Elderfield, H., 1988. The oceanic chemistry of the rare earth elements. Philos. Trans. R. Soc. London, A 325, 105–126.
Elderfield, H., Pagett, R., 1986. Rare earth elements in ichthyoliths: variations with redox conditions and depositional environment. Sci. Total Environ. 49, 175–197.
Eriksson, P.G., Condie, K.C., Tirsgaard, H., Mueller, W.U., Altermann, W., Miall, A.D., Aspler, L.B., Catuneanu, O., Chiarenzelli, J.R., 1998. Precambrian clastic sedimentation systems. Sediment. Geol. 120, 5–53.
Farquhar, J., Zerkle, A., Bekker, A., 2011. Geological constraints on the origin of oxygenic photosynthesis. Photosynth. Res. 107, 11–36.
Fischer, W.W., Schroeder, S., Lacassie, J.P., Beukes, N.J., Goldberg, T., Strauss, H., Horstmann, U.E., Schrag, D.P., Knoll, A.H., 2009. Isotopic constraints on the Late Archean carbon cycle from the Transvaal Supergroup along the western margin of the Kaapvaal Craton, South Africa. Precambrian Res. 169, 15–27.
Floran, R.J., Papike, J.J., 1978. Mineralogy and petrology of the Gunflint Formation, Minnesota-Ontario. J. Petrology 19, 215–288.

Flörke, O.W., Graetsch, H., Martin, B., Röller, K., Wirth, R., 1991. Nomenclature of microcrystalline and non-crystalline silica minerals, based on structure and microstructure. Neues Jahrbuch Für Mineralogie-Abhandlungen 163 (1), 19–42.
Folk, R.L., 1974. The natural history of crystalline calcium carbonate: effect of magnesium content and salinity. J. Sedim. Petrol. 44, 40–53.
Folk, R.L., Siedlecka, A., 1974. The "schizohaline" environment: Its sedimentary and diagenetic fabrics as exemplified by Late Paleozoic rocks of Bear Island. Svalbard. Sediment. Geol. 11, 1–15.
Fralick, P., 1989. Microbial bioherms, Lower Proterozoic Gunflint Formation, Thunder Bay, Ontario. In: Geldsetzer, H.H.J., James, N.P., Tebbutt, G.E. (Eds.), Reefs: Canada and Adjacent Areas. Canadian Society of Petroleum Geologists, Memoirs, pp. 24–29.
Fralick, P., Barrett, T., 1995. Depositional controls on iron formation associations in Canada. Spec. Pub. Int. Ass. Sediment. 22, 137–156.
Fralick, P., Davis, D., Kissin, S., 2002. The age of the Gunflint Formation, Ontario, Canada: single zircon U Pb age determinations from reworked volcanic ash. Can. J. Earth Sci. 39 (1091), 1085–1091. http://dx.doi.org/10.1139/E02-028.
Gallagher, K.L., Kading, T.J., Braissant, O., Dupraz, C., Visscher, P.T., 2012. Inside the alkalinity engine: the role of electron donors in the organomineralization potential of sulfate-reducing bacteria. Geobiology 10, 518–530.
Given, R.K., Lohmann, K.C., 1985. Derivation of the original isotopic composition of Permian marine cements. J. Sediment. Petrol. 55, 430–439.
Goodwin, A.M., 1956. Facies relations in the Gunflint Iron Formation. Econ. Geol. 51, 565–595.
Goodwin, A.M. 1960. Gunflint Formation of the Whitefish Lake area. In Ontario Department of Mines Annual Report 69, pp. 41–63.
Graetsch, H., 1994. Structural characteristics of opaline and micro-crystalline silica minerals. In: Heaney, P.J., Prewitt, C.T., Gibbs, G.V. (Eds.), Silica. Physical Behaviour, Geochemistry and Materials Applications, Reviews in Mineralogy, vol. 29, pp. 209–232.
Graetsch, H., Flörke, O.W., Miehe, G., 1987. Structural defects in microcrystalline silica. Phys. Chem. Minerals 14, 249–257.
Grotzinger, J.P., 1986. Evolution of Early Proterozoic passive-margin carbonate platform, Rocknest Formation, Wopmay Orogen, Northwest Territories, Canada. J. Sediment. Petrol. 56, 831–847.
Grotzinger, J.P., 1994. Trends in Precambrian carbonate sediments and their implication for understanding evolution. In: Bengston, S. (Ed.), Early Life on Earth: New York. Columbia University Press, pp. 245–258.
Grotzinger, J.P., Read, J.F., 1983. Evidence for primary aragonite precipitation, lower Proterozoic (1.9 Ga) Rocknest dolomite, Wopmay orogen. Northwest Canada. Geology 11, 710–713.
Hesse, R., 1989. Silica diagenesis: origin of inorganic and replacement cherts. Earth-Sci. Rev. 26, 253–284.
Hiatt, E.E., Pufahl, P.K., Edwards, C.T., 2015. Sedimentary phosphate and associated fossil bacteria in a Paleoproterozoic tidal flat in the 1.85Ga Michigamme Formation, Michigan, USA. Sediment. Geol. 319, 24–39.
Hofmann, H.J., Jackson, G.D., 1987. Proterozoic ministromatolites with radial-fibrous fabric. Sedimentology 34, 963–971.
Hollander, D.J., McKenzie, J.A., 1991. CO_2 control on carbon-isotope fractionation during aqueous photosynthesis: a paleo-pCO_2 barometer. Geology 19, 929–932.
House, C.H., Schopf, J.W., McKeegan, K.D., Coath, C.D., Harrison, T.M., Stetter, K.O., 2000. Carbon isotopic composition of individual Precambrian microfossils. Geology 28, 707–710.
Huang, C., 2010. Rare Earth Coordination Chemistry: Fundamentals and Applications. John Wiley & Sons (Asia), Singapore, p. 575.
Jirsa, M., Fralick, P., 2010. Geology of the Gunflint Iron Formation and the Sudbury Impact Layer, Northeastern Minnesota, Institute on Lake Superior Geology, Field Trip 4. Field Trip Guidebooks 53, 77–92.
Johannesson, K.H., Hawkins, D.L., Cortés, A., 2006. Do Archean chemical sediments record ancient seawater rare earth element patterns? Geochim. Cosmochim. Acta 70, 871–890.
Johannesson, K.H., Telfeyan, K., Chevis, D.A., Rosenheim, B.E., Leybourne, M.I., 2014. Rare earth elements in stromatolites-1. Evidence that modern terrestrial stromatolites fractionate rare earth elements during incorporation from ambient waters. In: Dilek, Y., Furnes, H. (Eds.), Evolution of Archean Crust and Early Life, Modern Approaches in Solid Earth Sciences 7. Springer Science+Business Media Dordrecht. http://dx.doi.org/10.1007/978-94-007-7615-9_14.
Jones, B., 2013. Microarchitecture of dolomite crystals as revealed by subtle variations in solubility: implications for dolomitization. Sediment. Geol. 288, 66–80.
Kamber, B.S., Webb, G.E., 2001. The geochemistry of late Archaean microbial carbonate: implications for ocean chemistry and continental erosion history. Geochim. Cosmochim. Acta 65, 2509–2525.
Kamber, B.S., Webb, G.E., 2007. Transition metal abundances in microbial carbonate: a pilot study based on *in situ* LA-ICP-MS analysis. Geobiology 5, 375–389. http://dx.doi.org/10.1111/j.1472-4669.2007.00129.x.
Kamber, B.S., Bolhar, R., Webb, G.E., 2004. Geochemistry of late Archaean stromatolites from Zimbabwe: evidence for microbial life in restricted epicontinental seas. Precambrian Res. 132, 379–399.
Kawabe, I., Ohta, A., Miura, N., 1999. Distribution coefficients Fe oxyhydroxide of REE between precipitates and NaCl solutions affected by REE complexation. Geochem. J. 33, 181–197.
Kenward, P.A., Goldstein, R.H., González, L.A., Roberts, J.A., 2009. Precipitation of low-temperature dolomite from an anaerobic microbial consortium: the role of methanogenic Archaea. Geobiology 7, 556–565.
Kershaw, S., 2015. Modern Black Sea oceanography applied to the end-Permian extinction event. J. Palaeogeogr. 4, 1–18.
Kershaw, S., Crasquin, S., Li, Y., Collin, P.-Y., Forel, M.-B., Mu, X., Baud, A., Wang, Y., Xie, S., Maurer, F., Guo, L., 2012. Microbialites and global environmental change across the Permian-Triassic boundary: a synthesis. Geobiology 10, 25–47.
Knauth, L.P., 1979. A model for the origin of chert in limestone. Geology 7, 274–277.
Knauth, L.P., 1994. Petrogenesis of chert. In: Heaney, P.J. et al. (Eds.), Silica: Physical Behavior, Geochemistry and Materials Applications. Mineralogical Society of America, vol. 29, pp. 233–258.
Knoll, A., 1985. Exceptional preservation of photosynthetic organisms in silicified carbonates and silicified peats. Philos. Trans. R. Soc. B 311, 111–122.
Knoll, A.H., 2003. Life on a Young Planet: the First Three Billion Years of Evolution on Earth. Princeton University Press, New Jersey.
Konhauser, K., Phoenix, V., 2001. Microbial–silica interactions in Icelandic hot spring sinter: possible analogues for some Precambrian siliceous stromatolites. Sedimentology 48, 415–433.
Konhauser, K.O., Jones, B., Phoenix, V.R., Ferris, G., Renaut, R.W., 2004. The microbial role in hot spring silicification. Ambio 33, 552–558.
Konhauser, K.O., Newman, D.K., Kappler, A., 2005. The potential significance of microbial Fe(III)-reduction during Precambrian banded iron formations. Geobiology 3, 167–177.
Konhauser, K.O., Lalonde, S.V., Planavsky, N.J., Pecoits, E., Lyons, T.W., Mojzsis, S.J., Rouxel, O.J., Barley, M.E., Rosière, C., Fralick, P.W., Kump, L.R., Bekker, A., 2011. Aerobic bacterial pyrite oxidation and acid rock drainage during the Great Oxidation Event. Nature 478, 369–373.
Lepot, K., Benzerara, K., Brown, G.E., Philippot, P., 2008. Microbially influenced formation of 2,724 million years old stromatolites. Nat. Geosci. 1, 118–121.
Lowe, D.R., 1983. Restricted shallow-water sedimentation of Early Archean stromatolitic and evaporitic strata of the Strelley Pool Chert, Pilbara Block, Western Australia. Precambrian Res. 19, 239–283.
Maliva, R.G., Knoll, A.H., Simonson, B.M., 2005. Secular change in the Precambrian silica cycle: insights from chert petrology. Geol. Soc. Am. Bull. 117, 835.
Marin, J., Chaussidon, M., Robert, F., 2010. Microscale oxygen isotope variations in 1.9 Ga Gunflint cherts: assessments of diagenesis effects and implications for oceanic paleotemperature reconstructions. Geochim. Cosmochim. Acta 74, 116–130.
Marin, J., Chaussidon, M., Robert, F., 2012. Micrometer-scale chemical and isotopic criteria (O and Si) on the origin and history of Precambrian cherts: implications for paleo-temperature reconstructions. Geochim. Cosmochim. Acta 92, 129–147.
Markun, C.D., Randazzo, A.F., 1980. Sedimentary structures in the Gunflint Iron Formation, Schreiber Beach, Ontario. Precambrian Res. 12, 287–310.
Mazzullo, S.J., 1980. Calcite pseudospar replacive ofmarine acicular aragonite, and implications for aragonite cement diagenesis. J. Sediment. Petrol. 50, 409–422.
Mojzsis, S.J., Arrhenius, G., 1998. Phosphates and carbon on Mars: exobiological implications and sample return considerations. J. Geophys. Res. 103, 28495–28511.
Mojzsis, S.J., Cates, N.L., Bleeker, W., Hopkins, M.D., Guitreau, M., Blichert-Toft, J., Trail, D., Abramov, O., 2014. Component geochronology of the ca. 3960 Ma Acasta Gneiss. Geochim. Cosmochim. Acta 133, 68–96.
Moorehouse, W.W. 1960. Gunflint Iron Range in the vicinity of Port Arthur. In Ontario Department of Mines Annual Report 69. pp. 1–40.
Moreau, J., Sharp, T., 2004. A transmission electron microscopy study of silica and kerogen biosignatures in ~1.9 Ga Gunflint microfossils. Astrobiology 4, 196–210.
Morse, J.W., Mackenzie, F.T., 1990. Geochemistry of Sedimentary Carbonates. Elsevier Science Publishers B.V, Amsterdam, p. 706.
Naafs, B.D.A., Castro, J.M., De Gea, G.A., Quijano, M.L., Schmidt, D.N., Pancost, R.D., 2016. Gradual and sustained carbon dioxide release during Aptian Oceanic Anoxic Event 1a. Nat. Geosci. 9, 135–139.
Nance, W.B., Taylor, S.R., 1976. Rare earth patterns and crustal evolution: I. Australian post-Archean sedimentary rocks. Geochim. Cosmochim. Acta 40, 1539–1551.
Nudds, J.R., Selden, P.A., 2008. Fossil Ecosystems of North America: A Guide to the Sites and Their Extraordinary Biotas. University of Chicago Press, Chicago, IL, p. 288.
Palmer, M.R., 1985. Rare earth elements in foraminifera tests. Earth Planet. Sci. Lett. 73, 285–298.
Palmer, M.R., Elderfield, H., 1986. Rare earth elements and neodym- ium isotopes in ferromanganese oxide coatings pf Cenozoic foram- inifera from the Atlantic Ocean. Geochim. Cosmochim. Acta 50, 409–417.
Papineau, D., Mojzsis, S.J., Coath, C.D., Karhu, J.A., McKeegan, K.D., 2005. Multiple sulfur isotopes of sulfides from sediments in the aftermath of Paleoproterozoic glaciations. Geochim. Cosmochim. Acta 69, 5033–5060.
Partin, C.A., Bekker, A., Planavsky, N.J., Lyons, T.W., 2015. Euxinic conditions recorded in the ca. 1.93 Ga Bravo Lake Formation, Nunavut (Canada): implications for oceanic redox evolution. Chem. Geol. 417, 48–162.
Petrash, D.A., Gingras, M.K., Lalonde, S.V., Orange, F., Pecoits, E., Konhauser, K.O., 2012. Dynamic controls on accretion and lithification of modern gypsum-dominated thrombolites, Los Roques, Venezuela. Sediment. Geol. 245–246, 29–47. http://dx.doi.org/10.1016/j.sedgeo.2011.12.006.
Picard, A., Obst, M., Schmid, G., Zeitvogel, F., Kappler, A., 2015. Limited influence of Si on the preservation of Fe mineral-encrusted microbial cells during experimental diagenesis. Geobiology. http://dx.doi.org/10.1111/gbi.12171.
Pittman Jr., J.S., Folk, R.L., 1971. Length-slow chalcedony after sulfate minerals in sedimentary rocks. Nat. Phys. Sci. 230, 64–65.

Planavsky, N., Rouxel, O., Bekker, A., Shapiro, R., Fralick, P., Knudsen, A., 2009. Iron-oxidizing microbial ecosystems thrived in late Paleoproterozoic redox-stratified oceans. Earth Planet. Sci. Lett. 286, 230–242.
Poulton, S.W., Fralick, P.W., Canfield, D.E., 2004. The transition to a sulphidic ocean similar to 1.84 billion years ago. Nature 431, 173–177.
Poulton, S.W., Fralick, P.W., Canfield, D.E., 2010. Spatial variability in oceanic redox structure 1.8 billion years ago. Nature Geosci. 3, 486–490.
Pufahl, P.K., 1996. Stratigraphic Architecture of a Paleoproterozoic iron formation depositional system: the Gunflint, Mesabi and Cuyuna iron ranges Master's of Science Thesis. Lakehead University, Thunder Bay, Ont.
Pufahl, P.K., and Fralick, P.W., 2000, Depositional environments of the Paleoproterozoic Gunflint Formation: in Institute on Lake Superior Geology Proceedings, 46 Annual Meeting, Thunder Bay, Ontario, Part 2 Field Trip Guidebook 51.
Raiswell, R., Fisher, Q.J., 2000. Mudrock-hosted carbonate concretions: a review of growth mechanism and their influence on chemical and isotopic composition. J. Geol. Soc. 157, 239–252.
Rasmussen, B., 1996. Early-diagenetic REE-phosphate minerals (florencite, gorceixite, crandallite, and xenotime) in marine sandstones; a major sink for oceanic phosphorus. Am. J. Sci. 296, 601–632.
Reynard, B., Lécuyer, C., Grandjeau, P., 1999. Crystal-chemical controls on rare earth element concentrations in fossil biogenic apatite and implications for paleoenvironmental reconstructions. Chem. Geol. 155, 233–242.
Riciputi, L.R., Paterson, B.A., Ripperdan, R.L., 1998. Measurement of light stable isotope ratios by SIMS: Matrix effects for oxygen, carbon, and sulfur isotopes in minerals. Int. J. Mass Spectrom. 178, 81–112.
Ricketts, B.D., 1983. The evolution of a middle Precambrian dolostone sequence: a spectrum of dolomitization regimes. SEPM J. Sediment. Res. 53, 565–586.
Riding, R., 2006. Cyanobacterial calcification, carbon dioxide concentrating mechanisms, and Proterozoic-Cambrian changes in atmospheric composition. Geobiology 4, 299–316.
Riding, R., Fralick, P., Liang, L., 2014. Identification of an Archean marine oxygen oasis. Precambrian Res. 251, 232–237.
Robbins, L.J., Swanner, E.D., Lalonde, S.V., Eickhoff, M., Paranich, M.L., Reinhard, C.T., Peacock, C.L., Kappler, A., Konhauser, K.O., 2015. Limited Zn and Ni mobility during simulated iron formation diagenesis. Chem. Geol. 402, 30–39.
Schopf, J.W., Packer, B.M., 1987. Early Archean (3.3-billion to 3.5-billion-year-old) micro-fossils from Warrawoona Group, Australia. Science 237, 70–73.
Schroeder, J.H., 1972. Fabrics and sequences of submarine carbonate cements in Holocene Bermuda cup reefs. Geol Rundsch 61, 708–730.
Shapiro, R.S., Konhauser, K.O., 2015. Hematite-coated microfossils: primary ecological fingerprint or taphonomic oddity of the Paleoproterozoic? Geobiology 13, 209–224.
Sheldon, N.D., 2006. Precambrian paleosols and atmospheric CO_2 levels. Precambrian Res. 147, 148–155.
Shields, G., Stille, P., 2001. Diagenetic constraints on the use of cerium anomalies as palaeoseawater redox proxies: an isotopic and REE study of Cambrian phosphorites. Chem. Geol. 175, 29–48.
Shinn, E.A., 1969. Submarine lithification of Holocene carbonate sediments in the Persian Gulf. Sedimentology 12, 109–144.
Sholkovitz, E.R., Shen, G.T., 1995. The incorporation of rare earth elements in modern coral. Geochim. Cosmochim. Acta 59, 2749–2756.
Sibley, D., Gregg, J., 1987. Classification of dolomite rock textures. J. Sediment. Res. 57, 967–975.
Siever, R., 1962. Silica solubility 0–200°C and the diagenesis of siliceous sediments. J. Geol. 70, 127–150.
Simonson, B.M., 1987. Early silica cementation and subsequent diagenesis in arenites from four Early Proterozoic iron formations in North America. J. Sed. Petrol. 57, 494–511.
Simonson, B.M., Hassler, S.W., 1996. Was the deposition of large Precambrian iron formations linked to major marine transgressions? J. Geol. 104, 665–676.
Simonson, B.M., Lanier, W.P., 1987. Early silica cementation and microfossil preservation in cavities in iron formation stromatolites, early Proterozoic of Canada. In: Appel, P.W.U., LaBerge, G.L. (Eds.), Precambrian iron formations. Theophratus Publications, Athens, pp. 187–213.
Sommers, M.G., Awramik, S.M., 1996. Abiogenic "stromatolites" from the Gunflint Formation: Microstructural criteria for determining abiogenic vs. biogenic stromatolites. Abstracts Programs, Geol. Soc. Am. 28 (7), 174.
Sommers, M.G., Awramik, S.M., Woo, K.S., 2000. Evidence for initial calcite-aragonite composition of Lower Algal Chert Member ooids and stromatolites, Paleoproterozoic Gunflint Formation, Ontario, Canada. Can. J. Earth Sci. 1243, 1229–1243.
Stille, P., Clauer, N., 1986. Sm-Nd isochron-age and provenance of the argillites of the Gunflint Iron Formation in Ontario, Canada. Geochim. Cosmochim. Acta 50, 1141–1146.
Strauss, H., Moore, T.B., 1992. Abundances and isotopic compositions of carbon and sulfur species in whole rock and kerogen samples. In: Schopf, J.W., Klein, C. (Eds.), The Proterozoic Biosphere. Cambridge University Press, Cambridge, pp. 709–798.
Taylor, S.R., McLennan, S.M., 1985. The Continental Crust: Its Composition and Evolution. Blackwell, Malden, MA.
Taylor, T.N., Taylor, E.L., 1993. The Biology and Evolution of Fossil Plants. Prentice Hall, New Jersey, USA, p. 384.
Tyler, S.A., Barghoorn, E.S., 1963. Ambient pyrite grains in Precambrian cherts. Am. J. Sci. 261, 424–432.
Van Kranendonk, M.J., Webb, G.E., Kamber, B.S., 2003. New geological and trace element evidence from 3.45 Ga stromatolitic carbonates in the Pilbara Craton: support of a marine, biogenic origin and for a reducing Archaean ocean. Geobiology 1, 91–108.
Veizer, J., Clayton, R.N., Hinton, R.W., 1992. Geochemistry of Precambrian carbonates: IV. Early Paleoproterozoic (2.25 ± 0.25 Ga) seawater. Geochim. Cosmochim. Acta 56 (3), 875–885.
Wacey, D., Kilburn, M.M.R., Saunders, M., Cliff, J., Brasier, M.D., 2011. Microfossils of sulphur-metabolizing cells in 3.4-billion-year-old rocks of Western Australia. Nat. Geosci. 4, 1–5.
Wacey, D., Menon, S., Green, L., Gerstmann, D., 2012. Taphonomy of very ancient microfossils from the ~3400Ma Strelley Pool Formation and ~1900Ma Gunflint Formation: new insights using a focused ion beam. Precambrian Res. 220–221, 234–250.
Wacey, D., McLoughlin, N., Kilburn, M.R., Saunders, M., Cliff, J.B., Kong, C., Barley, M. E., Brasier, M.D., 2013. Nanoscale analysis of pyritized microfossils reveals differential heterotrophic consumption in the ~1.9-Ga Gunflint chert. Proc. Natl. Acad. Sci. U.S.A. 110, 8020–8024.
Wahl, C., Miehe, G., Fuess, H., 2002. TEM characterisation and interpretation of fabric and structural degree of order in microcrystalline SiO_2 phases. Contrib. Mineral. Petrol. 143, 360–365.
Walter, M.R., 1972. Stromatolites and the biostratigraphy of the Australian Precambrian and Cambrian. Spec. Pap. Palaeontol. 11, 1–190.
Webb, G.E., Kamber, B.S., 2000. Rare earth elements in Holocene reefal microbialites: a new shallow seawater proxy. Geochim. Cosmochim. Acta 64, 1557–1565.
Winter, B.L., Knauth, L.P., 1992. Stable isotope geochemistry of cherts and carbonates from the 2.0 Ga Gunflint Iron Formation: implications for the depositional setting, and the effects of diagenesis and metamorphism. Precambrian Res. 59, 283–313.